https://doi.org/10.5194/egusphere-2026-7050
Preprint. Discussion started: 24 November 2026
© Author(s) 2026. CC BY 4.0 License.

Reconciling SWOT Altimetry, Tide Gauges, and Sea-Level Fields from a Regional Ocean Forecasting System in the Baltic Sea

Niyousha Nikbakhsh[1], Amirhossein Barzandeh[1], Priidik Lagemaa[1], and Urmas Raudsepp[1]
[1]Department of Marine Systems, Tallinn University of Technology, Tallinn, Estonia
Correspondence: Niyousha Nikbakhsh (niyousha.nikbakhsh@taltech.ee)

Abstract. Time-varying offsets uniform over single passes within sub-basins can dominate the disagreement between Surface Water and Ocean Topography (SWOT) sea level and a regional Baltic Sea forecast. Using three years of SWOT observations, 56 tide gauges and the Copernicus Marine Baltic forecast, we develop a framework that separates static, time-varying and spatially structured discrepancies and assesses what satellite and coastal observations each contribute. Apart from the datum offset, the time-varying component accounts for 66% of the mean-square difference, while a static offset field and a spatially structured residual, correlated over about 60 km, each contribute 17%. Triple collocation with the gauges, assuming independent errors, attributes 41% of the variance of the time-varying component to model error that the gauges see. Testing all 16 combinations of base anomaly and corrections shows that the dynamic atmospheric correction and ocean tide must be restored to the SWOT anomaly. With both restored, the unfiltered anomaly is the robust default for the Level-3 product version tested, with a centred root-mean-square difference of 4.73 cm against the gauges and 6.60 cm against the model. The denoised anomaly agrees slightly better where it works but failed, unflagged, on one coastal pass. Cross-validated on alternate repeat cycles, static and gauge-based corrections reduce the datum-adjusted SWOT–model root-mean-square difference from 7.21 to 5.29 cm. If the SWOT error of 4.14 cm at the gauges from triple collocation holds offshore and is independent of the model error, about 3.29 cm of model error remains. The framework quantifies what gauge-based corrections can remove and establishes a benchmark for testing joint assimilation of SWOT and tide gauges.

1 Introduction

Sea level in coastal and shelf seas is observed mainly at tide gauges along the coast and by nadir altimeters offshore. Gridded altimetry resolves wavelengths of 100–200 km at mid-latitudes (Fu and Ubelmann, 2014; Dufau et al., 2016; Ballarotta et al., 2019), which is coarse compared with narrow gulfs, straits and archipelagos. The Surface Water and Ocean Topography (SWOT) mission, launched in December 2022, maps sea surface height across two swaths of about 50 km on either side of a 20 km nadir gap with the Ka-band Radar Interferometer (KaRIn) (Morrow et al., 2019; Fu et al., 2024), with errors at scales below 100 km two to four times smaller than anticipated before launch (Wang et al., 2025), although valid samples become scarce within a few kilometres of the coast (Kupavõh et al., 2024). For shelf seas this provides two-dimensional sea level fields against which regional models can be validated and eventually corrected. SWOT and tide gauges are complementary in this respect,

https://doi.org/10.5194/egusphere-2026-7050
Preprint. Discussion started: 24 November 2026
© Author(s) 2026. CC BY 4.0 License.

since the gauges observe sea level continuously but only at the coast, whereas SWOT observes it offshore in two dimensions but only at the times of its passes.

Comparing SWOT with a model requires a sea level that contains the same physical signals as the model. The SWOT Level-3 Expert product provides a sea surface height anomaly, unfiltered and denoised with a neural network, together with the geophysical corrections removed from it (Tréboutte et al., 2023; AVISO/DUACS, 2024; Dibarboure et al., 2025). These are the dynamic atmospheric correction (DAC), which combines the high-frequency barotropic response to wind and pressure from a global model with the inverse barometer at periods longer than 20 days (Carrère and Lyard, 2003; Carrere et al., 2016), the ocean tide from FES2022 (Lyard et al., 2021; CNES, 2024) and the coherent internal tide (Zaron, 2019; Zaron and Elipot, 2024). Adding a correction back restores the observed signal, whereas leaving it removed keeps only what the correction model missed. Nadir Level-3 products are distributed in the same way, with the removed corrections provided separately (Pujol et al., 2016; Taburet et al., 2019; Pujol et al., 2023; AVISO/DUACS, 2026), and for a model forced by wind and pressure and including tides the guidance is to re-inject the DAC, the ocean tide and the internal tide (Pujol et al., 2023).

In practice the choice has been made implicitly and differently for each purpose. Studies of storm surges kept the signal that the DAC removes (Han et al., 2012; Antony et al., 2014; Vega-Gimenez et al., 2025), total water level was rebuilt with the tide and the atmospheric terms on the north-west European shelf (Rulent et al., 2020) and in the hyper-tidal Bristol Channel (Lichtman et al., 2025; Rong et al., 2026), and in the Baltic the DAC was added back to nadir and SWOT data (Mostafavi et al., 2023, 2024; Esselborn et al., 2025). Other studies moved the corrections to the reference, removing the DAC and the tide from tide gauges (Cheng et al., 2018; Sánchez-Román et al., 2020; Zhu et al., 2025) or applying atmospheric corrections to gauges and models (Zhai et al., 2025; Fouchet et al., 2025). These studies rarely quantified the contribution of each term, so it remains unclear how much of the reported agreement is owed to the corrections and whether a choice that served one region holds in another.

A single answer is not to be expected, because the formula depends on which processes dominate sea level in a basin and on how well the global correction models represent them there. In macro-tidal settings the tide carries most of the variance, and tide models can err by tens of centimetres near complex coasts (Hart-Davis et al., 2024), while the internal tide correction matters only where internal tides are generated or propagate (Carrere et al., 2021; Yadidya et al., 2025; Tchilibou et al., 2025). In microtidal seas the atmospheric terms dominate, yet in the Gulf of Genoa most of the DAC was the inverse barometer (Picco et al., 2020), whereas Baltic sea level responds to wind as much as to air pressure (Samuelsson and Stigebrandt, 1996; Leppäranta and Myrberg, 2009), and the skill of the global DAC model varies between regions (Pascual et al., 2008). The assessment therefore has to be made basin by basin and for the processes each model contains.

The Baltic Sea is a demanding case for this choice, and each switch raises its own question there. Sea level is driven mainly by wind and air pressure through storm surges, seiches and the exchange through the Danish straits (Samuelsson and Stigebrandt, 1996; Leppäranta and Myrberg, 2009; Weisse et al., 2021), and coastal water level variability and its extremes differ strongly between sub-basins (Soomere et al., 2018; Männikus et al., 2020; Männikus and Soomere, 2023; Viigand et al., 2025; Leszczyńska et al., 2025). Most of the synoptic signal is therefore expected in the DAC. If the DAC is left removed, SWOT keeps only the part of this signal that the global model behind the DAC, driven by fields of the European Centre for

https://doi.org/10.5194/egusphere-2026-7050
Preprint. Discussion started: 24 November 2026
© Author(s) 2026. CC BY 4.0 License.

Medium-Range Weather Forecasts (ECMWF), did not reproduce (AVISO/DUACS, 2026), whereas a regional model responds to its own atmospheric forcing (Müller et al., 2017; Lindenthal et al., 2025). Astronomical tides are significant only in the Kattegat and Skagerrak (Medvedev et al., 2016), so the ocean tide should matter there and little elsewhere. The internal tide correction is an empirical model derived from nadir altimetry (Zaron, 2019; Zaron and Elipot, 2024; AVISO/DUACS, 2026), and whether it contributes anything in a shallow, semi-enclosed sea is not known. The base anomaly is uncertain as well, because the internal Rossby radius is a few kilometres (Fennel et al., 1991), whereas the denoising may affect features shorter than 50 km and strong filtering can remove dynamical signal (Tréboutte et al., 2023; AVISO/DUACS, 2026; Demol et al., 2026). Nadir altimetry has described Baltic sea level variability and trends (Madsen et al., 2007; Stramska, 2013; Passaro et al., 2021), and the first SWOT studies compared Level-2 data with geoid-referenced gauges (Kupavõh et al., 2024), described the 2023 Major Baltic Inflow (Esselborn et al., 2025) and validated the marine geoid (Schwabe et al., 2026), but none tested which corrections should be re-injected.

A model cannot decide between these formulas, because its own errors would favour the formula that resembles the model rather than the sea. Tide gauges record total sea level independently of the corrections and of the model, and they are the standard reference for coastal altimetry (Cipollini et al., 2017; Vignudelli et al., 2019; Noubissie et al., 2024). They lie at the coast, however, where valid SWOT samples are scarce (Kupavõh et al., 2024), so we also determine up to what distance from a gauge SWOT still agrees with it. The three data sets refer to different vertical datums, SWOT to a mean sea surface, the gauges to national height systems that differ by a few centimetres (Kollo and Ellmann, 2019; Varbla et al., 2022; Schwabe et al., 2026) and the model to a zero level set by its open boundary, with biases of tens of centimetres (Kärnä et al., 2021; Jandt-Scheelke et al., 2024). We therefore compare variability with each record's own mean removed, and use absolute levels only in the comparison with the model, to separate a static offset from the parts that vary.

Once the formula is fixed, the difference between SWOT and a model still has to be interpreted. Product validation usually reports how closely SWOT matches tide gauges or a model, and sometimes an error estimate for SWOT itself (e.g., Kupavõh et al., 2024; Zhu et al., 2025; Han et al., 2026), but rarely what the disagreement with a model consists of, which part of it is model error and whether the gauges already see that error, and these decide how SWOT can be used with a model. A bias, fixed or slowly varying, can be removed by post-processing (Jahanmard et al., 2023), whereas errors in the simulated dynamics call for correcting the model state through data assimilation (Madsen et al., 2015; Le Traon et al., 2025), which Baltic operational systems do not apply to sea level (Fu et al., 2012; Axell and Liu, 2016; Lindenthal et al., 2025). Which of the two separates SWOT from a Baltic model decides which remedy is worth developing. Tide gauges already measure part of the model error continuously at the coast, so the value of SWOT for a model lies in the model error that the gauges miss, which only a joint diagnosis of the three data sets can locate. Swath altimetry has improved global forecasts when assimilated (Benkiran et al., 2026), but it can guide such a choice only if its own errors are known as well.

This study develops an integrated diagnosis of the disagreement between SWOT, tide gauges and a regional model in the Baltic Sea, and asks what the satellite and the coastal observations each contribute to it. It proceeds in two steps. First, we write the SWOT Level-3 sea level as a linear formula in which the base anomaly and each removed correction are switched on or off, derive a criterion for when re-injecting a correction improves the agreement, and test every switch against tide gauges for

https://doi.org/10.5194/egusphere-2026-7050
Preprint. Discussion started: 24 November 2026
© Author(s) 2026. CC BY 4.0 License.

Table 1. Data sets used in this study.

Data set	Product, dataset and DOI	Variables used	Sampling and coverage
SWOT Level-3 Expert v3.0	AVISO/DUACS `L3_LR_SSH` Expert, 10.24400/527896/A01-2023.018 (AVISO/DUACS, 2024)	Anomalies, corrections, MDT, quality flag	2 km swath grid, science cycles 3–55
Tide gauges	`INSITU_BAL_PHYBGCWAV_DISCRETE_MYNRT_013_032`, 10.48670/moi-00032 (E.U. Copernicus Marine Service Information, 2026a)	Water surface height above station datum	Hourly or 10 min
Model sea level	`BALTICSEA_ANALYSISFORECAST_PHY_003_006`, `cmems_mod_bal_phy_anfc_PT15M-i`, 10.48670/moi-00010 (E.U. Copernicus Marine Service Information, 2026b)	`sla` and land–sea mask	15 min, about 1 nautical mile

the whole basin, each sub-basin and each gauge. The criterion needs only tide gauges and the variables distributed with the product, so the test can be repeated in other basins. Second, we compare SWOT with the 15-min sea level of the Copernicus Marine Baltic forecast and split their difference into a static offset, an offset uniform over a sub-basin that varies in time and a part that varies in space within a sub-basin, because each part calls for a different remedy. We then use the tide gauges as a third data set to attribute the time-varying offset to SWOT and to the model, and test retrospectively how much of the difference offset corrections remove, which sets a benchmark for more advanced corrections.

2 Data and methods

2.1 Study area and data

The study area is the Baltic Sea including the Danish straits, the Kattegat and the Skagerrak, between ~9°E and ~30°E and between ~53°N and ~66°N, the domain of the regional model (Lindenthal et al., 2025). It is divided into seven sub-basins following Leppäranta and Myrberg (2009), the Skagerrak and Kattegat, the western Baltic, the Baltic Proper, the Gulf of Riga, the Gulf of Finland, the Bothnian Sea and the Bothnian Bay. The study period is 1 September 2023 to 31 August 2026, three years of the SWOT science phase with its 20.86-day repeat orbit (science cycles 3 to 55). Table 1 lists the data sets. All times are in UTC.

2.2 SWOT Level-3 sea level

SWOT sea level is taken from the `L3_LR_SSH` Expert product, version 3.0 (AVISO/DUACS, 2024; Dibarboure et al., 2025). We use the reprocessed series up to 1 May 2025 and the forward series afterwards, which are calibrated against delayed-time and near-real-time nadir altimetry, respectively, so that a small offset can occur at their junction (AVISO/DUACS, 2026). Of the 59 passes that cross the study area in each cycle, 3034 files were available for the 53 cycles, each on a 2 km grid of 69 cross-track pixels (Table 2). Only samples with `quality_flag` equal to zero are used, which excludes samples flagged for sea ice,

https://doi.org/10.5194/egusphere-2026-7050
Preprint. Discussion started: 24 November 2026
© Author(s) 2026. CC BY 4.0 License.

Table 2. SWOT Level-3 Expert variables used in this study.

Variable	Content	Use in this study
`ssha_unfiltered`	Anomaly with all corrections, calibration and editing applied	Base anomaly U
`ssha_filtered`	As above after U-Net denoising	Base anomaly F
`dac`	High-frequency barotropic response to ECMWF wind and pressure plus inverse barometer at periods longer than 20 days	Re-injected or not
`ocean_tide`	Geocentric FES2022 ocean tide including load tide and long-period tides	Re-injected or not
`internal_tide`	Coherent internal tide, HRET22	Re-injected or not
`mdt`	Mean dynamic topography, HYBRID-CNES-CLS22-CMEMS2020	Absolute dynamic topography
`quality_flag`	Editing class	Only good samples
`cross_track_distance`	Distance from nadir	Swath position

rain, coastal contamination, outliers and the swath edges (AVISO/DUACS, 2026), and undefined values of `internal_tide` are set to zero.

Every SWOT sea level considered here is a case of

$$\eta_S = \text{ssha_filtered} + \delta_U\,(\text{ssha_unfiltered} - \text{ssha_filtered}) + \delta_D\,\text{dac} + \delta_T\,\text{ocean_tide} + \delta_I\,\text{internal_tide}, \tag{1}$$

where each switch δ is one or zero. The switch δ_U selects the base anomaly, and δ_D, δ_T and δ_I re-inject the DAC, the ocean tide and the internal tide. The two anomalies have the same corrections removed and differ only in the denoising, so either can serve as the base. Equation (1) gives 16 formulas, named by the base anomaly, F or U, and the re-injected terms, for example U+DAC+OT for $\delta_U = \delta_D = \delta_T = 1$ and $\delta_I = 0$, and the generic formula for a model forced by wind and pressure and including tides (Pujol et al., 2023) is F+DAC+OT+IT. The data-driven calibration of instrument errors (Dibarboure et al., 2022) is kept in all formulas. To split the difference between SWOT and the model, the formula is completed to absolute dynamic topography with the mean dynamic topography (MDT) of the product, which carries a deliberate offset of -5 cm (AVISO/DUACS, 2026),

$$\eta_A = \eta_S + \text{mdt}. \tag{2}$$

2.3 Tide gauges and the regional model

Tide gauge records are taken from the Copernicus Marine Baltic in situ product (E.U. Copernicus Marine Service Information, 2026a), 240 records in the study area. We keep values flagged as good or probably good, remove values more than 3 m from the record median, runs of identical values longer than 3 h and isolated spikes of more than 20 cm, average records sampled more often than every 10 min to 10-min values, and require good data in at least half of the hours. Of two records less than 2 km apart only the longer is kept, and possible datum changes are flagged by comparing daily means with the best-correlated neighbouring gauges. Storm-surge days are the days on which the average hourly anomaly of the gauges of a sub-basin exceeds its 99th percentile, extended by one day on either side, 39 to 81 of the 1096 days depending on the sub-basin.

https://doi.org/10.5194/egusphere-2026-7050
Preprint. Discussion started: 24 November 2026
© Author(s) 2026. CC BY 4.0 License.

Model sea level is the 15-min instantaneous sea level (`sla`) of the Copernicus Marine Baltic Sea Physics Analysis and Forecast (E.U. Copernicus Marine Service Information, 2026b), a system based on the Nucleus for European Modelling of the Ocean (NEMO) (Hordoir et al., 2019; Kärnä et al., 2021; Madec et al., 2024) with a resolution of about one nautical mile. It is forced by wind and pressure from the 2.5 km MetCoOp-HARMONIE system, receives tides through its open boundaries and does not assimilate sea level (Müller et al., 2017; Lindenthal et al., 2025; Jandt-Scheelke et al., 2024), so it is independent of SWOT and of the gauges. Its code changed from NEMO 4.0.4 to 4.2.1 on 26 November 2024 (Lindenthal et al., 2025). For the comparison with the gauges, model and gauge records are averaged to hourly values, with the model at the sea cell nearest to each gauge.

2.4 Collocation and anomaly frame

For every gauge and pass we take the valid SWOT pixel nearest to the gauge within 5 km (Esselborn et al., 2025) and the gauge value nearest in time within 30 min. A pixel is valid if all terms of Eq. (1) are defined, if it lies more than 1 km from the nearest land cell of the model grid and if it lies in the sub-basin of the gauge, connected to it by water. All formulas are evaluated on identical collocations without interpolation. A gauge is used if it has a model sea cell within 5 km, at least 20 collocations and a correlation of at least 0.80 with the best of the 16 formulas, which removes gauges in lagoons and river mouths without favouring any formula, and of gauges closer than 10 km only the one with the most collocations is kept. For the comparison with the model, we take for every pass and sea cell the valid SWOT pixel nearest to the cell centre and the model sea level at the nearest 15-min time, and use cells with at least 20 collocations.

All statistics use anomalies. For a gauge or model cell j and the set $\mathcal{C}_j$ of times at which it is collocated with SWOT, the anomaly of any variable x is

$$x'_j(t) = x_j(t) - \frac{1}{|\mathcal{C}_j|} \sum_{\tau \in \mathcal{C}_j} x_j(\tau), \tag{3}$$

computed separately for each data set over the same times, so that datum offsets and differences in sampling cannot bias the comparison. A change of reference within the period, at the junction of the SWOT series or at the model upgrade, is tested at the gauges as the change in the mean SWOT minus gauge or model minus gauge difference, and a significant change would split the records.

2.5 Metrics and significance

We compute the centred root-mean-square difference (cRMSD), the Pearson correlation r, the ratio of standard deviations and the mean absolute difference (MAE) between anomalies. For SWOT and a reference R, the tide gauges (G) or the model (M), with standard deviations σ_S and σ_R,

$$\mathrm{cRMSD}^2 = (\sigma_S - \sigma_R)^2 + 2\sigma_S\sigma_R(1 - r) \tag{4}$$

(Taylor, 2001), which splits the squared cRMSD into an amplitude part and a part due to timing and spatial pattern. Each sub-basin receives the same total weight, so that the densely instrumented western Baltic does not dominate the pooled values.

https://doi.org/10.5194/egusphere-2026-7050
Preprint. Discussion started: 24 November 2026
© Author(s) 2026. CC BY 4.0 License.

Confidence intervals come from 1000 bootstrap resamples of whole days, which keep all passes of a day together (Künsch, 1989; Efron and Tibshirani, 1993), and the same resamples are used for all formulas, so that their differences are paired and significant when the 95% interval excludes zero. The daily mean SWOT minus gauge and model minus gauge differences decorrelate within one day and the pass offsets of Sect. 2.6 within one to six days, and resampling blocks of 7 or 21 days widens the intervals by up to 1.82 times without changing any conclusion (Table S1 in the Supplement). Sea level statistics are given in centimetres with two decimals, that is to 0.1 mm, so that differences between formulas of a millimetre or less remain visible. Such differences are reported with their confidence intervals, and even where significant they are small compared with the errors of SWOT and the model.

Because Eq. (1) is linear, the effect of each switch follows directly. Let η_S be a formula without the term X and η_G the gauge sea level. Switching X on gives

$$\mathrm{cRMSD}^2(\eta_S + X) = \mathrm{cRMSD}^2(\eta_S) - \sigma_X^2\,(2\beta_X - 1), \qquad \beta_X = \frac{\mathrm{cov}(X', \eta_G' - \eta_S')}{\sigma_X^2}, \tag{5}$$

where σ_X is the standard deviation of the term and β_X the regression coefficient of the residual $\eta_G' - \eta_S'$ on it. Re-injecting a term therefore improves the agreement only if $\beta_X > 1/2$. A value of one means that the correction reproduces the observed signal it represents with the right amplitude, and a value of zero that re-injecting it only adds its variance. Switching on two terms X and Y changes the squared cRMSD by the sum of the single changes plus $2\,\mathrm{cov}(X', Y')$, so nearly uncorrelated terms contribute additively. Each switch is tested for the whole basin, each sub-basin and each gauge, and the ranking is repeated for 23 subsets and variants by season, storm-surge days, cross-track distance, weighting, time difference and without the gauges flagged for a datum change. The collocation is also repeated for the nearest valid pixel in rings from 0–2 to 25–30 km around each gauge.

2.6 Static, time-varying and spatially varying differences

Let $d = \eta_A - \eta_M$ be the difference between SWOT absolute dynamic topography and the model sea level η_M at a collocation in model cell j, pass p and sub-basin k. It is split sequentially as

$$d = c + (\bar{d}_j - c) + u_{pk} + \varepsilon, \tag{6}$$

where c is the overall mean of d, $\bar{d}_j$ its time mean in cell j, u_{pk} the mean of $d - \bar{d}_j$ over pass p in sub-basin k and ε the remainder. The constant c reflects the vertical datums, $\bar{d}_j - c$ is a static offset field, u_{pk} an offset uniform over a pass and sub-basin that changes from pass to pass, and ε a residual that varies in space within a pass and sub-basin. Their mean squares add up to that of $d - c$ apart from two cross-products of the static part that cancel, and the sequential shares are compared with the reverse order and with a joint least-squares fit of the static and uniform parts.

The model is then corrected along a ladder (L) of steps of increasing complexity, numbered L1 to L5, where L refers to the ladder and not to the processing level of satellite products. After each step the root-mean-square difference (RMSD) to η_A is computed, for a constant offset (L1), a static offset per cell (L2), in addition a time-varying sub-basin offset measured at the tide gauges (L3), and in addition the remaining offset of each pass and sub-basin (L4). The gauge-based offset is the hourly

https://doi.org/10.5194/egusphere-2026-7050
Preprint. Discussion started: 24 November 2026
© Author(s) 2026. CC BY 4.0 License.

model minus gauge anomaly, the median over the gauges of each sub-basin smoothed with a centred 25 h running mean, and does not use SWOT, whereas L4 uses SWOT itself and is the best any offset correction can achieve. A scaling of the model anomaly per cell added to L3 (L5) and two statistical corrections, the gauge-based offset with a fitted coefficient and a ridge regression on the gauge-based offsets of all sub-basins, are tested in addition.

Every correction except L4 is estimated on the odd cycles and applied to the even cycles, and vice versa, so that it is credited only with what it removes on cycles not used to estimate it. The constant and the static offsets of L1 to L3 are therefore means over the other half of the cycles, in cells with at least 10 collocations there. The test is nevertheless retrospective and not a forecast test, because the two halves interleave over the whole record and the centred running mean of the gauge-based offset uses gauge data up to 12 h after each time. A real-time application would need a trailing window and an offset carried over the forecast lead time, which were not tested. The shares of Eq. (6), in contrast, describe the whole record.

2.7 Errors of SWOT, the model and the tide gauges

SWOT, the gauge and the model of the gauge cell are available together at the gauge collocations, and their error variances are estimated by triple collocation, which assumes mutually independent errors (Stoffelen, 1998; McColl et al., 2014). The results are error variances under this model, and their sensitivity to an assumed error covariance between each pair of data sets is tested. The SWOT and gauge errors so obtained include representation error, from a pixel up to 5 km away and from a point compared with a model cell (Oke and Sakov, 2008; Janjić et al., 2018).

The uniform part is attributed at the level of the pass offsets. We write $u_{pk} = a_{pk} - b_{pk}$, with a_{pk} the SWOT error and b_{pk} the model error uniform over pass p and sub-basin k, and use the gauge-based model offset g_{pk} at the same samples as a third data set. If the errors of SWOT and of the gauges are independent of each other and of the model errors, triple collocation gives $\sigma_b^2 = \mathrm{cov}(u_{pk}, -g_{pk})$, where σ_b is the standard deviation of b_{pk}, provided the model error at the gauges equals that offshore. Otherwise this is the part of the model error that the gauges also see, and model error that they miss is counted as SWOT error. Lower bounds on σ_b under weaker assumptions are derived in Sect. S1 of the Supplement. The uniform part is also regressed on the mean DAC anomaly of the pass and sub-basin to test for an error in the amplitude of the DAC.

The model is also compared hourly with all gauges that passed the quality control. Its error is split with centred running means into variations slower than 30 days, between 2 and 30 days and faster than 2 days, and the part common to a sub-basin is estimated at each gauge from the other gauges of the sub-basin, with the same centred 25 h running mean. The spatial structure of the differences is described by structure functions, the mean squared difference between two collocations of the same pass and sub-basin against their separation, which at zero separation give twice the variance of spatially uncorrelated noise (Hollingsworth and Lönnberg, 1986). Within a pass and sub-basin the uniform part cancels, so the structure function of the SWOT minus model anomaly describes ε.

https://doi.org/10.5194/egusphere-2026-7050
Preprint. Discussion started: 24 November 2026
© Author(s) 2026. CC BY 4.0 License.

Table 3. SWOT formulas of Eq. (1) against the tide gauges for the nearest valid pixel within 5 km, 56 gauges and 4087 collocations, with the switches of each formula. cRMSD and difference to the best formula in cm, with 95% confidence intervals from resampling whole days, correlation and ratio of standard deviations. Formulas with $\delta_I = 1$ are identical to those listed, because `internal_tide` is zero or undefined in the Baltic.

Formula	δ_U	δ_D	δ_T	cRMSD	r	σ_S/σ_G	ΔcRMSD to best
F	0	0	0	13.70 (12.96, 14.37)	0.69	0.79	8.97 (8.27, 9.65)
F+OT	0	0	1	12.89 (12.15, 13.59)	0.73	0.82	8.16 (7.44, 8.87)
F+DAC	0	1	0	8.42 (7.70, 9.19)	0.90	1.03	3.69 (3.01, 4.44)
F+DAC+OT	0	1	1	7.25 (6.43, 8.11)	0.93	1.06	2.52 (1.73, 3.38)
U	1	0	0	12.55 (11.96, 13.17)	0.74	0.73	7.82 (7.23, 8.43)
U+OT	1	0	1	11.66 (11.07, 12.25)	0.78	0.77	6.93 (6.38, 7.51)
U+DAC	1	1	0	6.39 (6.08, 6.68)	0.94	0.99	1.65 (1.45, 1.87)
U+DAC+OT	1	1	1	4.73 (4.42, 5.07)	0.97	1.02	–

3 Results

3.1 Collocations with the tide gauges

Of the 240 gauge records, 154 passed the quality control. SWOT passes within 5 km of 152 of them, a median of 206 times, but only 60 reach 20 collocations with a valid pixel, because valid KaRIn samples are scarce near the coast, in archipelagos and in fjords (Fig. 1a). The correlation test removed three German gauges in a fjord and in the Szczecin Lagoon area, and Dragor was removed in favour of Drogden, 7.36 km away. The 56 gauges used cover all sub-basins (Fig. 1b, c) and provide 4087 collocations, 20 to 191 per gauge, with a valid pixel at a median of 38% of the overpasses and none in the Bothnian Bay from about December to May because of sea ice. The offset at the junction of the reprocessed and forward SWOT series, -0.04 cm (-0.80 to 0.60 cm), and the model step at its upgrade, -0.53 cm (-2.14 to 1.23 cm), are not significant, so neither record was split.

3.2 Choice of the SWOT formula

The `internal_tide` variable is zero or undefined at every collocation, so δ_I has no numerical effect and the 16 formulas reduce to eight (Table 3, Fig. 2). This shows that the distributed correction is inactive in the Baltic, not that the physical internal tide is zero. The cRMSD ranges from 13.70 cm for F to 4.73 cm for U+DAC+OT, every other formula is significantly worse than U+DAC+OT, and the generic formula F+DAC+OT+IT is third with 7.25 cm. Without the DAC, SWOT has only 0.73 to 0.82 of the standard deviation of the gauges, and with it 0.99 to 1.06.

The ranking follows from Eq. (5) (Table 4). Each term changes the squared cRMSD by almost the same amount whatever the other switches, by 113.66 to 116.87 cm^2 for the DAC, 18.34 to 21.56 cm^2 for the ocean tide and 30.09 to 30.16 cm^2 for the base anomaly, because the terms are nearly uncorrelated. The regression coefficient β_X is 0.96 to 0.98 for the DAC and 1.00

https://doi.org/10.5194/egusphere-2026-7050
Preprint. Discussion started: 24 November 2026
© Author(s) 2026. CC BY 4.0 License.

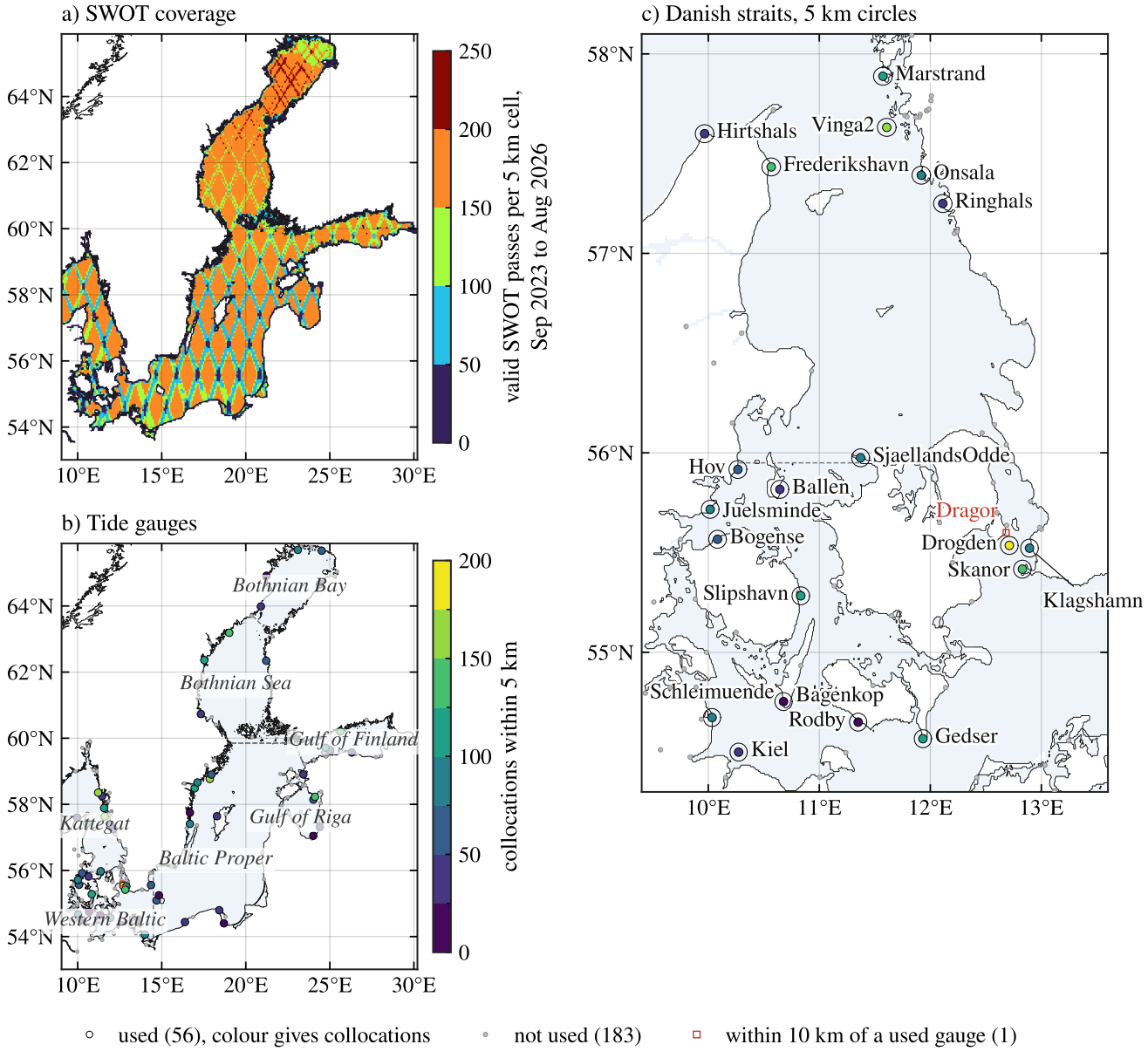

Figure 1. (a) Number of passes with a valid SWOT sample in each 5 km cell from September 2023 to August 2026. (b) Tide gauges used, coloured by the number of collocations within 5 km, gauges not used (grey) and the gauge removed because a used gauge lies within 10 km (red square). Dashed lines separate the sub-basins. (c) The Danish straits with the 5 km circles around the gauges used.

to 1.09 for the ocean tide, so neither correction has a large systematic amplitude error. The DAC, with a standard deviation of 11.07 cm, improves the agreement significantly in every sub-basin, from 4.35 cm in the Bothnian Sea to 9.96 cm in the

https://doi.org/10.5194/egusphere-2026-7050
Preprint. Discussion started: 24 November 2026
© Author(s) 2026. CC BY 4.0 License.

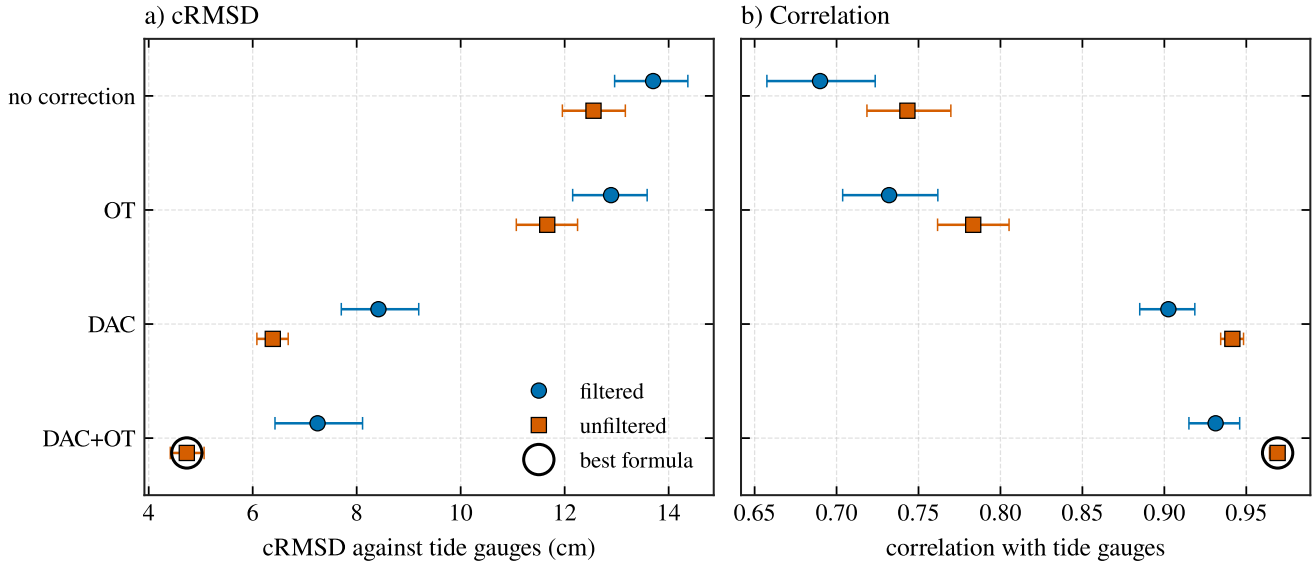

Figure 2. (a) cRMSD and (b) correlation between SWOT and the tide gauges for the filtered (circles) and the unfiltered (squares) anomaly with each set of re-injected corrections, with 95% confidence intervals. Formulas with the internal tide are identical and not shown. The ring marks the formula with the lowest cRMSD.

Table 4. Contribution of each switched term of Eq. (1) to the selected formula U+DAC+OT, for the DAC, the ocean tide (OT), the internal tide (IT) and the part of the unfiltered anomaly removed by the denoising (U−F). Standard deviation σ_X of the term (cm), regression coefficient β_X of the gauge residual on the term and reduction of the squared cRMSD (cm^2) from Eq. (5), and change in cRMSD (cm) when the term is switched off, or for δ_I switched on, for all gauges with 95% confidence interval. The next columns give the number of gauges at which this switch makes the agreement significantly worse, not significantly different (n.s.) and significantly better, and the median and range of the change over the 56 gauges. Positive changes mean that the setting of U+DAC+OT is the better choice.

Term	σ_X	β_X	$\sigma_X^2 \times (2\beta_X - 1)$	All	Worse	n.s.	Better	Per gauge
DAC (δ_D)	11.07	0.96	113.66	6.93 (6.38, 7.51)	55	1	0	7.01 (1.61, 13.53)
OT (δ_T)	4.28	1.00	18.39	1.65 (1.45, 1.87)	36	20	0	0.78 (−0.38, 9.70)
IT (δ_I)	0.00	–	0.00	0.00 (0.00, 0.00)	0	56	0	0.00 (0.00, 0.00)
U−F (δ_U)	5.36	1.02	30.13	2.52 (1.73, 3.38)	1	40	15	−0.08 (−0.72, 22.08)

Bothnian Bay (Fig. 3a), at 55 of the 56 gauges, and by 10.33 cm on storm-surge days against 6.57 cm on other days. The ocean tide, with a standard deviation of 4.28 cm, gains most in the Skagerrak and Kattegat (3.72 cm) and the western Baltic (3.02 cm) and is not significant in the Bothnian Sea (Fig. 3b). It improves the agreement significantly at 36 gauges, by up to 9.70 cm at Hov, and worsens it at none.

https://doi.org/10.5194/egusphere-2026-7050
Preprint. Discussion started: 24 November 2026
© Author(s) 2026. CC BY 4.0 License.

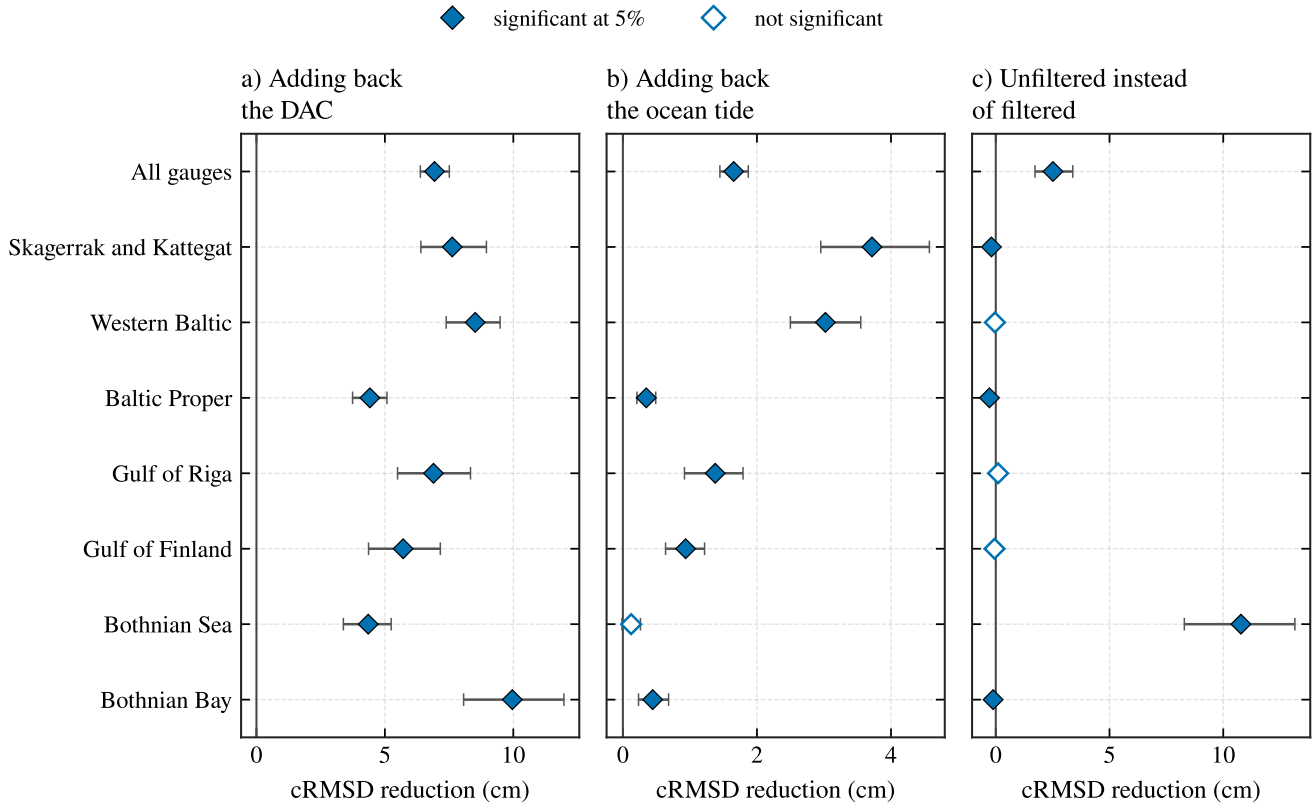

Figure 3. Reduction in cRMSD for all gauges and per sub-basin from (a) re-injecting the DAC (U+OT to U+DAC+OT), (b) re-injecting the ocean tide (U+DAC to U+DAC+OT) and (c) using the unfiltered instead of the filtered anomaly (F+DAC+OT to U+DAC+OT), with 95% confidence intervals. Filled symbols are significant at 5%.

Switching δ_U on lowers the pooled cRMSD by 2.52 cm, but this result comes from one gauge. At Spikarna in the Bothnian Sea, F+DAC+OT departs from the gauge with a cRMSD of 27.88 cm and U+DAC+OT with 5.80 cm. From November 2024 pass 29 gives there a filtered anomaly 18 to 96 cm below the unfiltered one on all 27 collocations, at a pixel 4.59 km from the gauge, close to land and about 16 km from nadir, which the quality flag does not mark (Fig. S1). The unfiltered anomaly of this pass also departs more from the gauge than on other passes, with a standard deviation of 7.59 against 4.22 cm, so the pixel itself is degraded and the denoising amplifies the error. Without these collocations and one similar collocation at Smögen, F+DAC+OT agrees better with the gauges than U+DAC+OT by 0.08 cm (0.04 to 0.12 cm), less than a millimetre, and the filtered anomaly is significantly better at 15 of the other 55 gauges, by 0.22 to 0.72 cm (Fig. 3c). The gauges thus determine which corrections to re-inject but not the base anomaly. We retain the unfiltered anomaly because it is never worse than the filtered one by more than 0.72 cm at any gauge, whereas the filtered anomaly failed without a flag. The SWOT sea level selected

https://doi.org/10.5194/egusphere-2026-7050
Preprint. Discussion started: 24 November 2026
© Author(s) 2026. CC BY 4.0 License.

for the Baltic is therefore

$$\boxed{\eta_S = \mathrm{ssha_unfiltered} + \mathrm{dac} + \mathrm{ocean_tide}}, \tag{7}$$

with δ_I free. Equation (7), completed with the MDT through Eq. (2), is used in the rest of the paper, and F+DAC+OT is evaluated alongside it against the model.

With U+DAC+OT the correlation at the individual gauges ranges from 0.91 to 0.99 and the cRMSD from 2.82 to 9.25 cm, with medians of 0.97 and 4.40 cm (Fig. S2, Table S3). U+DAC+OT is the best formula, or not significantly worse than the best, in 18 of the 23 subsets and variants, and in the other five F+DAC+OT is better by 0.09 to 0.28 cm. The nearest valid pixel agrees with a gauge as well as the 5 km collocation up to 6 km from the gauge, and every ring beyond 6 km is significantly worse (Fig. S3, Table S4), irregularly so, with the largest losses at 6–8 and 10–15 km, and partly because of real sea level differences, since the hourly anomalies of two gauges 10 to 30 km apart differ by 3.66 to 5.64 cm.

3.3 SWOT against the model

SWOT and the model were collocated 13.47 million times, and 119 738 of the 147 134 sea cells have at least 20 collocations (Fig. 4d). SWOT from Eq. (7) and the model agree with a cRMSD of 6.60 cm (6.34 to 6.85 cm), a correlation of 0.94 and a ratio of standard deviations of 1.02 (Table 5). The amplitude difference contributes 0.34% of the squared cRMSD and less than 5% in every sub-basin, so the two data sets differ in timing and spatial pattern rather than in variance. The cRMSD is lowest in the Baltic Proper and the Bothnian Sea, 4.78 and 4.90 cm, and highest in the Skagerrak and Kattegat, 9.23 cm (Fig. 4a). It decreases from 7.57 cm within 6 km of the coast to 5.65 cm beyond 50 km, and it is 8.11 cm in winter against 5.35 cm in summer and 8.74 cm on storm-surge days against 6.46 cm on other days.

Offshore the filtered anomaly gives the same agreement, within 0.02 cm beyond 6 km from the coast, whereas within 6 km it is worse by 0.67 cm (0.53 to 0.82 cm). Extrapolated to zero separation, the structure functions of SWOT give an uncorrelated noise of up to 0.94 cm for the unfiltered and 0.58 cm for the filtered anomaly, and the structure function of the unfiltered anomaly minus the model, 1.33 cm^2 at 1.74 km, gives a tighter bound of 0.81 cm for the unfiltered anomaly (Fig. 5). These noise levels are far below the 6.60 cm difference between SWOT and the model.

3.4 Static, time-varying and spatially varying differences

Apart from a constant of 43.75 cm, which reflects the vertical datums, the difference between SWOT absolute dynamic topography and the model has a standard deviation of 7.22 cm. Two thirds of its mean square (66%, 5.88 cm) is an offset uniform over a pass and sub-basin, one sixth (17%, 2.93 cm) a static offset field and one sixth (17%, 3.00 cm) varies in space within a pass and sub-basin (Table 6). The two cross-products of the static part are $\pm 0.62\%$ of the mean square, and the joint least-squares fit gives 16, 67 and 17%. Removing the uniform part first gives 7, 75 and 18%, because pass means then absorb part of the static field of the cells each pass samples. The uniform part dominates in every sub-basin, from 51% in the western Baltic to 81% in the Bothnian Bay, and beyond 6 km from the coast, whereas within 6 km the static part (38%) is as large as the

https://doi.org/10.5194/egusphere-2026-7050
Preprint. Discussion started: 24 November 2026
© Author(s) 2026. CC BY 4.0 License.

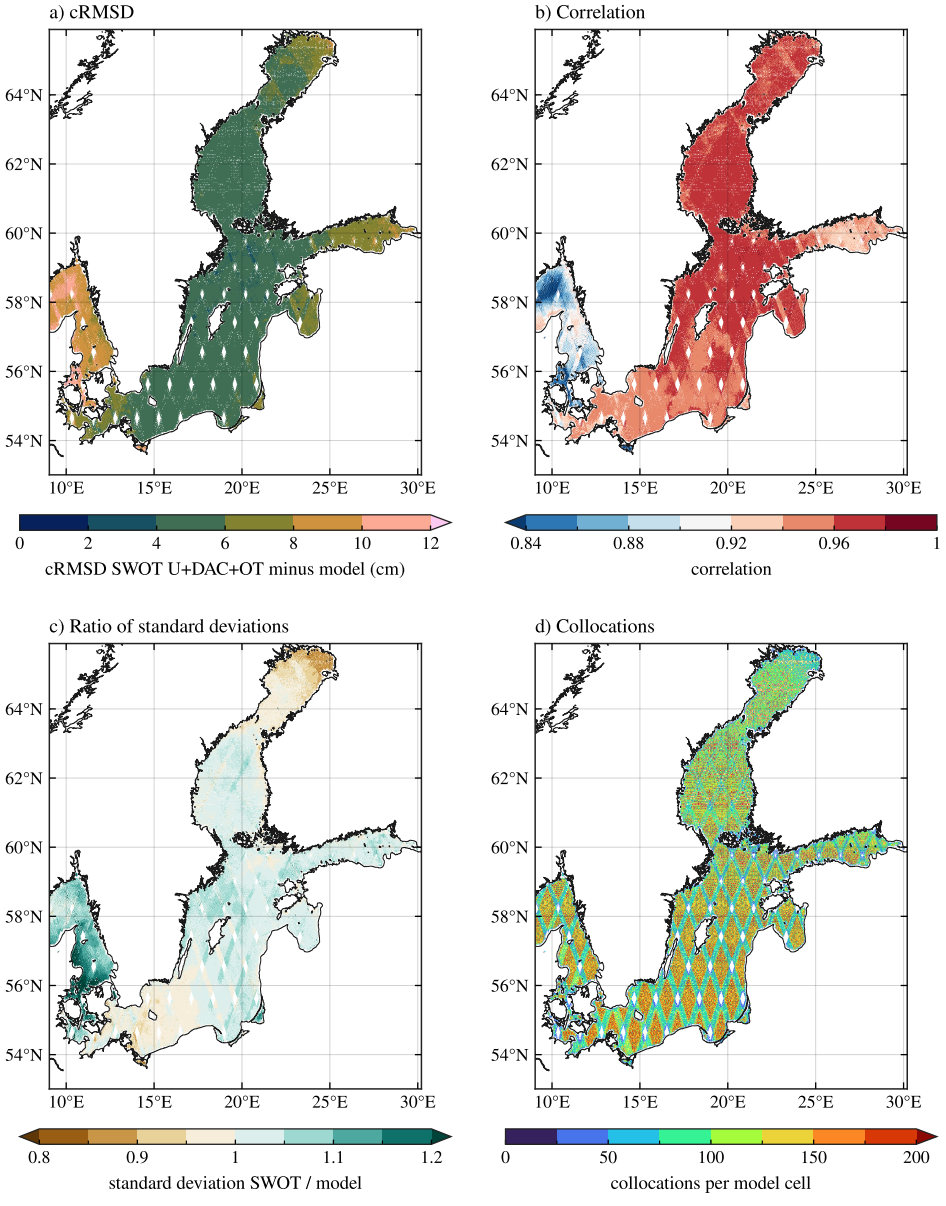

Figure 4. SWOT (U+DAC+OT) against the model per model cell. (a) cRMSD, (b) correlation, (c) ratio of the standard deviations of SWOT and the model and (d) number of collocations. White sea areas have fewer than 20 collocations.

295 uniform part (37%) and the residual reaches 25%. The static offset varies by about ±5 cm, with SWOT higher than the model in the central Baltic and the Bothnian Sea and lower in the Gulfs of Finland and Riga and the northern Bothnian Bay (Fig. 6a).

The uniform offsets change from pass to pass with a standard deviation of 6.00 cm and follow the model offset measured at the tide gauges (Fig. 7). Over 4293 pass and sub-basin means they correlate at 0.65 with the gauge minus model difference,

https://doi.org/10.5194/egusphere-2026-7050
Preprint. Discussion started: 24 November 2026
© Author(s) 2026. CC BY 4.0 License.

Table 5. SWOT (U+DAC+OT) against the model for the whole area, distance to the coast and sub-basins. cRMSD (cm) with 95% confidence interval, correlation, ratio of standard deviations, MAE (cm), share of the squared cRMSD due to the amplitude difference (%), and cRMSD of F+DAC+OT minus that of U+DAC+OT (cm) with 95% confidence interval.

Class	cRMSD	r	σ_S/σ_M	MAE	Amplitude	F − U
All	6.60 (6.34, 6.85)	0.94	1.02	4.90	0.34	0.06 (0.04, 0.08)
0–6 km	7.57 (7.30, 7.83)	0.92	1.02	5.23	0.21	0.67 (0.53, 0.82)
6–10 km	6.99 (6.72, 7.25)	0.94	1.02	5.23	0.42	0.01 (0.00, 0.02)
10–20 km	6.69 (6.43, 6.94)	0.95	1.02	5.03	0.41	0.02 (−0.01, 0.05)
20–50 km	6.46 (6.18, 6.75)	0.95	1.02	4.83	0.31	0.01 (−0.01, 0.04)
>50 km	5.65 (5.29, 6.01)	0.95	1.02	4.14	0.29	0.00 (−0.01, 0.02)
Skagerrak and Kattegat	9.23 (8.55, 10.02)	0.89	1.10	7.08	4.16	0.00 (−0.01, 0.00)
Western Baltic	6.98 (6.64, 7.31)	0.92	1.01	5.19	0.13	0.24 (0.18, 0.31)
Baltic Proper	4.78 (4.53, 5.02)	0.96	1.02	3.69	0.64	−0.02 (−0.02, −0.01)
Gulf of Riga	6.23 (5.67, 6.76)	0.96	1.03	4.80	1.00	0.07 (0.00, 0.17)
Gulf of Finland	6.96 (6.41, 7.48)	0.94	1.03	5.20	0.72	0.03 (0.01, 0.05)
Bothnian Sea	4.90 (4.53, 5.29)	0.97	1.02	3.71	0.51	0.02 (−0.01, 0.04)
Bothnian Bay	6.07 (5.61, 6.49)	0.96	0.95	4.62	4.03	0.07 (0.01, 0.15)

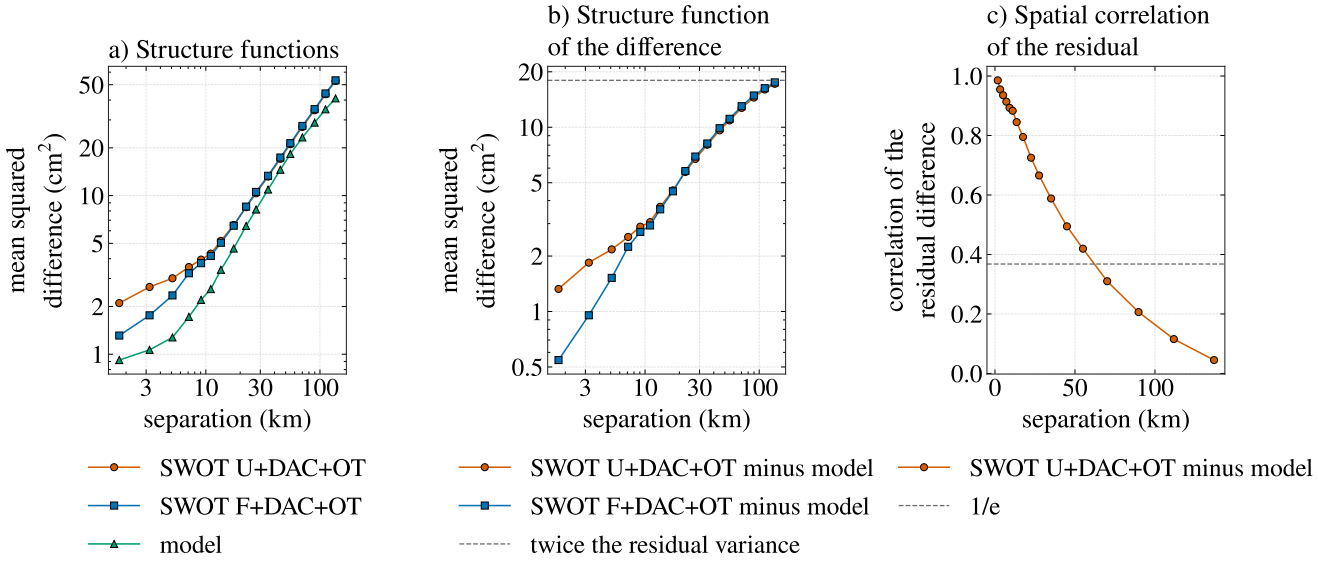

Figure 5. (a) Structure functions of SWOT (U+DAC+OT and F+DAC+OT) and the model, the mean squared difference between two collocations of the same pass and sub-basin against their separation. (b) Structure functions of SWOT minus the model, with twice the residual variance (dashed). (c) Spatial correlation of the residual SWOT minus model difference.

https://doi.org/10.5194/egusphere-2026-7050
Preprint. Discussion started: 24 November 2026
© Author(s) 2026. CC BY 4.0 License.

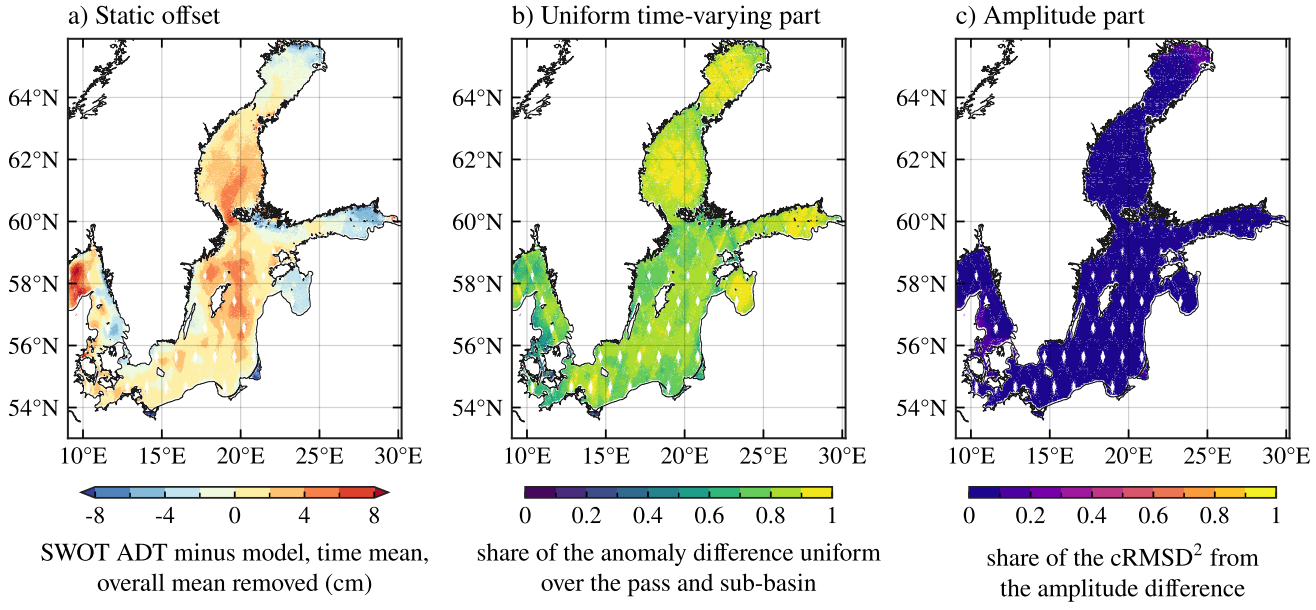

Figure 6. (a) Static offset between SWOT absolute dynamic topography and the model, with the overall mean removed. (b) Share of the SWOT minus model anomaly that is uniform over the pass and sub-basin. (c) Share of the squared cRMSD due to the amplitude difference.

from 0.49 in the western Baltic to 0.76 in the Bothnian Bay. Although the offsets decorrelate within one to six days on average, offsets of the same sign persist for weeks in some episodes in both series, as in January and February 2024 and in February 2025, and offsets beyond 10 cm occur in 9% of the cases, most often from November to February. The offsets are nearly uncorrelated with the mean DAC anomaly of the pass and sub-basin, with $r = 0.13$ and at most 0.26 in the Bothnian Sea.

The corrections reduce the RMSD step by step (Table 6, Fig. 8). After the constant offset it is 7.21 cm. The static offset per cell lowers it by 0.55 cm (0.46 to 0.62 cm) to 6.66 cm, the gauge-based offset by a further 1.38 cm (1.19 to 1.56 cm) to 5.29 cm, and the remaining offset of each pass and sub-basin to 3.03 cm. Scaling the model amplitude changes nothing (5.30 cm). On independent cycles the gauge-based offset explains 42% of the variance of the pass offsets, with or without a fitted coefficient, and a regression on the gauge-based offsets of all sub-basins 38%. The ordering of the steps holds in every sub-basin and distance class, and after all offsets the difference remains largest within 6 km of the coast (4.82 cm), in the Skagerrak and Kattegat (4.74 cm) and in the western Baltic (4.21 cm).

3.5 Errors of SWOT, the model and the tide gauges

At the 4087 gauge collocations SWOT is closer to the gauges than the model, with a cRMSD of 4.73 against 5.97 cm, a difference of 1.24 cm (0.90 to 1.60 cm) (Table 7). Triple collocation attributes an error of 4.14 cm (3.85 to 4.43 cm) to SWOT, 5.50 cm (5.17 to 5.80 cm) to the model and 2.29 cm (1.71 to 2.79 cm) to the gauges (Fig. 9a). The model error exceeds the SWOT error in the Skagerrak and Kattegat, the western Baltic and the Gulf of Finland, the two are similar in the Baltic Proper,

https://doi.org/10.5194/egusphere-2026-7050
Preprint. Discussion started: 24 November 2026
© Author(s) 2026. CC BY 4.0 License.

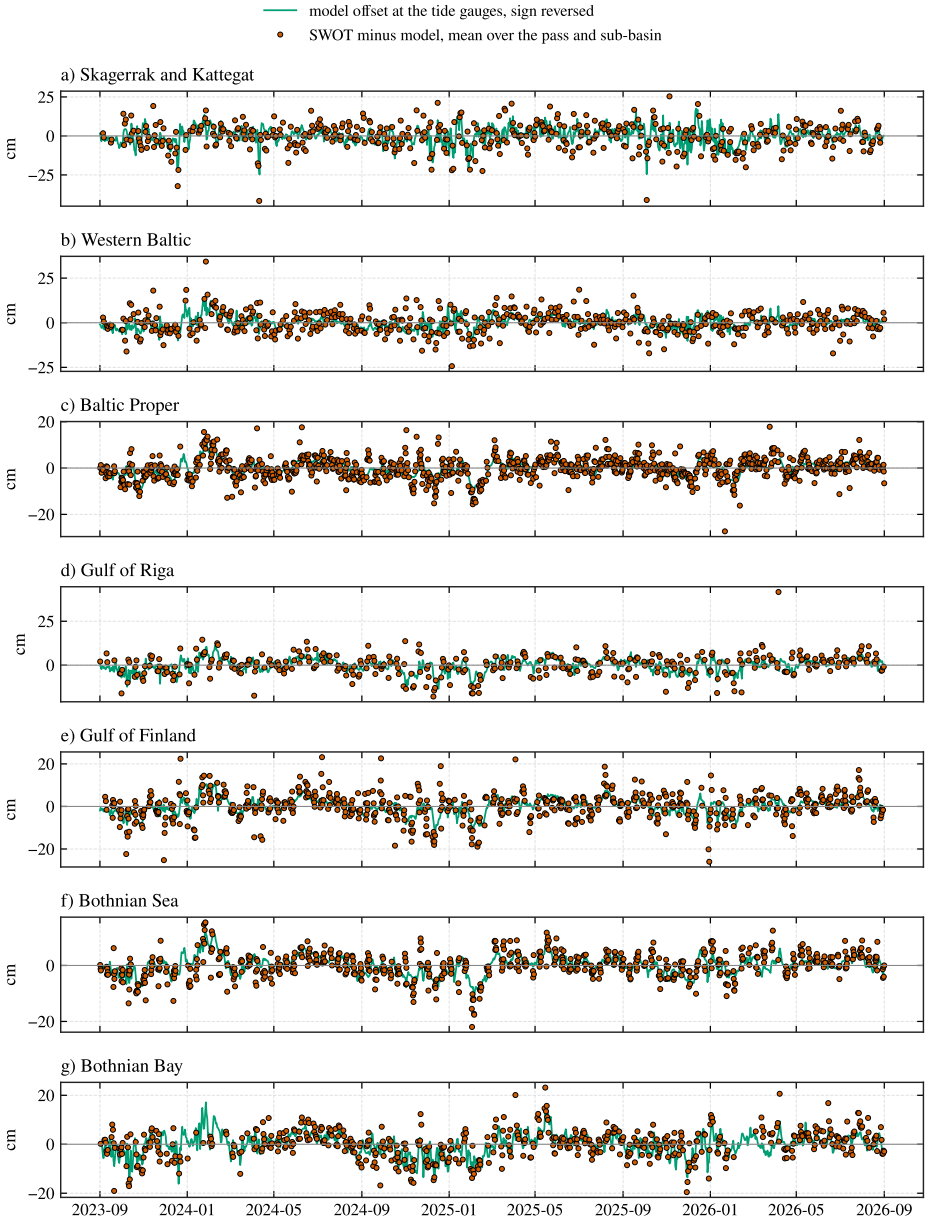

Figure 7. Mean SWOT minus model anomaly over each pass in each sub-basin (dots) and the model offset measured at the tide gauges of the sub-basin with reversed sign (line, daily means).

315 the Gulf of Riga and the Bothnian Bay, and in the Bothnian Sea the model error is smaller. With F+DAC+OT the SWOT error rises to 6.87 cm because of Spikarna. The gauge error variance is negative in the two Bothnian basins, but a gauge–model error covariance of 1.09 and 1.38 cm^2 removes this and changes the SWOT error to 4.64 and 4.09 cm and the model error to

https://doi.org/10.5194/egusphere-2026-7050
Preprint. Discussion started: 24 November 2026
© Author(s) 2026. CC BY 4.0 License.

Table 6. Parts of the difference between SWOT absolute dynamic topography (U+DAC+OT) and the model as shares of its mean square (%, rounded) after the constant datum offset of 43.75 cm is removed, and the RMSD (cm) after each correction. L1 removes the constant offset, L2 a static offset per cell, L3 in addition the time-varying sub-basin offset measured at the tide gauges, and L4 in addition the remaining offset of each pass and sub-basin estimated from SWOT. The shares describe the whole record, whereas L1 to L3 are estimated on one half of the cycles and evaluated on the other (Sect. 2.6).

	Share of mean square (%)			RMSD after correction (cm)			
Class	Static	Uniform	Residual	L1	L2	L3	L4
All	17	66	17	7.21	6.66	5.29	3.03
0–6 km	38	37	25	9.51	7.63	6.55	4.82
6–10 km	14	65	21	7.56	7.07	5.76	3.55
10–20 km	12	72	17	7.13	6.76	5.35	2.95
20–50 km	13	73	15	6.92	6.52	5.07	2.67
>50 km	24	63	13	6.47	5.71	4.36	2.31
Skagerrak and Kattegat	14	64	22	9.94	9.34	7.49	4.74
Western Baltic	21	51	28	7.80	7.05	6.57	4.21
Baltic Proper	19	65	16	5.30	4.81	3.66	2.18
Gulf of Riga	15	76	10	6.75	6.33	4.61	2.18
Gulf of Finland	16	73	11	7.56	7.01	5.57	2.54
Bothnian Sea	28	61	10	5.78	4.93	3.64	1.88
Bothnian Bay	8	81	11	6.33	6.10	4.18	2.12

4.02 and 5.24 cm, which leaves their comparison unchanged. For all gauges together the model error exceeds the SWOT error unless the SWOT and gauge errors share a covariance of more than 6.64 cm^2, a correlation of 0.40 (Fig. S4). Pixels within 2 km of a gauge and 2 to 5 km away give nearly the same SWOT error, 4.07 and 4.16 cm.

Triple collocation of the pass offsets with the gauge-based offset gives a model error of 3.85 cm and a SWOT error of 4.60 cm, so the model error that the gauges also see accounts for 41% of the variance of the offsets (36 to 46% from resampling 21-day blocks), from 28% in the western Baltic to 55% in the Bothnian Bay (Table S2, Fig. S5). If the SWOT and model errors are independent, the whole model part is at least 38% when the SWOT error is bounded by the SWOT minus gauge cRMSD, and at least 52% when it is bounded by the SWOT error from triple collocation at the gauges (Sect. S1). The second bound applies if the SWOT error uniform over a pass is not larger than the SWOT error at a single pixel, and it implies that model error of the order of a tenth of the variance of the offsets is not seen by the gauges.

Hourly against all 154 gauges, the model has a cRMSD of 3.62 to 13.52 cm with a median of 6.27 cm and a median correlation of 0.95, with the largest errors, 11.16 to 13.52 cm, in fjords and enclosed waters such as at Oslo, Hobro and Uddevalla, in the Kattegat and the Danish straits, and at St Petersburg. Errors faster than 2 days make up 55% of the error variance, with a standard deviation of 4.55 cm against 8.57 cm for the gauge signal in the same band, whereas slower errors are small relative to the signal, 3.01 against 11.97 cm between 2 and 30 days and 2.87 against 14.52 cm beyond 30 days (Fig. 9b,

https://doi.org/10.5194/egusphere-2026-7050
Preprint. Discussion started: 24 November 2026
© Author(s) 2026. CC BY 4.0 License.

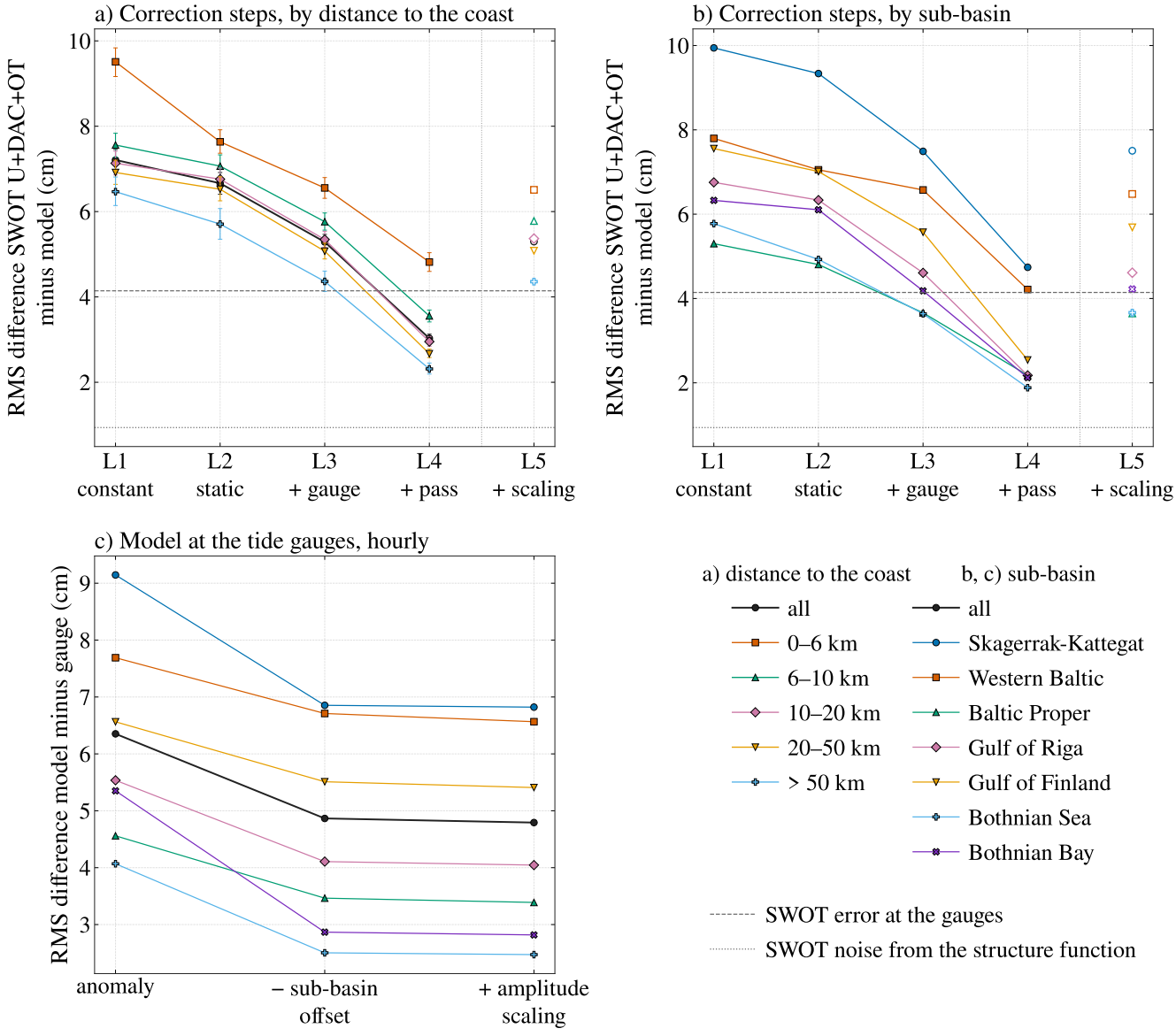

Figure 8. RMSD between SWOT absolute dynamic topography and the model after successive corrections (a) by distance to the coast, with 95% confidence intervals, and (b) by sub-basin. Open symbols on the right show the static and gauge-based offsets with amplitude scaling instead of the pass offset. Horizontal lines mark the SWOT error at the tide gauges from triple collocation and the uncorrelated SWOT noise. (c) RMSD between the model and the tide gauges, hourly, for the anomalies, after removing the sub-basin offset estimated from the other gauges and after amplitude scaling.

Table S5). The offset estimated from the other gauges removes 72% of the slow and 67% of the synoptic error variance but only 12% of the fast errors, and lowers the RMSD between model and gauges from 6.35 to 4.87 cm (Fig. 8c).

https://doi.org/10.5194/egusphere-2026-7050
Preprint. Discussion started: 24 November 2026
© Author(s) 2026. CC BY 4.0 License.

Table 7. SWOT (U+DAC+OT), tide gauges and model at the 4087 gauge collocations. Number of collocations, cRMSD of SWOT and of the model against the gauges, and the error standard deviation of each data set from triple collocation (cm), with 95% confidence intervals for SWOT and the model. A negative error variance is shown as the negative square root of its absolute value.

		cRMSD against gauge			Error standard deviation	
Group	n	SWOT	Model	Gauge	SWOT	Model
All	4087	4.73	5.97	2.29	4.14 (3.85, 4.43)	5.50 (5.17, 5.80)
Skagerrak and Kattegat	891	5.95	8.46	3.96	4.44 (3.50, 5.34)	6.98 (5.73, 8.18)
Western Baltic	1184	4.83	7.74	2.77	3.96 (3.44, 4.42)	7.03 (6.44, 7.61)
Baltic Proper	766	3.66	4.13	1.30	3.43 (3.05, 3.77)	3.80 (3.45, 4.11)
Gulf of Riga	251	4.40	5.07	1.67	4.07 (3.47, 4.64)	4.78 (4.11, 5.31)
Gulf of Finland	338	5.19	6.07	3.30	3.95 (3.31, 4.49)	5.06 (4.40, 5.63)
Bothnian Sea	396	4.64	3.73	−1.07	4.75 (4.17, 5.29)	3.87 (3.41, 4.30)
Bothnian Bay	261	4.09	4.97	−1.19	4.26 (3.49, 4.99)	4.76 (4.04, 5.35)

The residual difference between SWOT and the model is spatially correlated (Fig. 5). Its correlation stays above 0.80 up to about 15 km and falls below $1/e$ at 62 km, and its structure function approaches twice the residual variance at about 140 km. Although SWOT and the model have the same temporal variance, the model has less spatial variance within a pass and sub-basin at all separations, by 1.18 cm^2 at 1.74 km, of the order of the SWOT noise, and by 11.76 cm^2 at 136.93 km.

4 Discussion

4.1 A SWOT sea level for shelf-sea models

In the Baltic, the SWOT Level-3 sea level for comparison with a regional model is the unfiltered anomaly with the DAC and the ocean tide re-injected, Eq. (7). Re-injecting the DAC is the decisive step. Its coefficient of 0.96 rules out a large systematic amplitude error of the DAC, though not errors uncorrelated with it, so leaving it out discards observed signal rather than noise. The ocean tide matters where tides are significant (Medvedev et al., 2016) and degraded the agreement at no gauge, so it can be re-injected everywhere. The generic recommendation (Pujol et al., 2023) thus reduces in the Baltic to the DAC and the ocean tide, because the distributed internal tide correction is inactive there. The same is expected in other enclosed seas with small tides, but given the basin dependence discussed below it should be confirmed there with the same test.

The base anomaly is a choice between a slightly better fit and robustness. Where the denoising (Tréboutte et al., 2023) works, the filtered anomaly agrees with the gauges 0.08 cm better, but it failed by up to a metre on one coastal pass without a flag, and within 6 km of the coast it agrees less well even with the model, whose smoother field would favour a smoothed anomaly. Offshore the noise of the unfiltered anomaly is below 1 cm at the 2 km pixel scale, consistent with the low KaRIn noise found in the calibration phase (Wang et al., 2025) and far below the differences between SWOT and the model, so the denoising gains nothing measurable for a model with a resolution of about 2 km. The unfiltered anomaly is therefore the robust

https://doi.org/10.5194/egusphere-2026-7050
Preprint. Discussion started: 24 November 2026
© Author(s) 2026. CC BY 4.0 License.

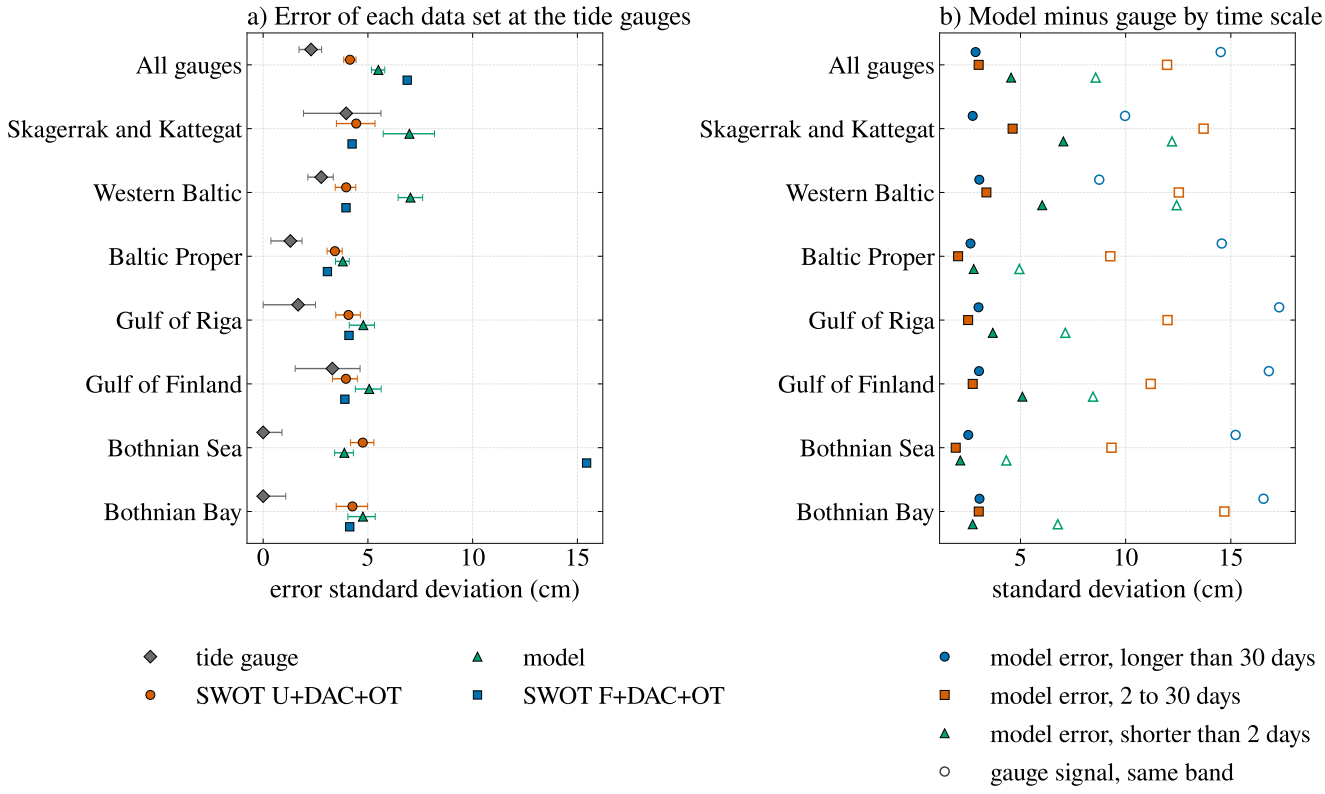

Figure 9. (a) Error standard deviation of the tide gauges, SWOT (U+DAC+OT and F+DAC+OT) and the model at the gauge collocations from triple collocation, with 95% confidence intervals. (b) Error of the model against the tide gauges (filled) and standard deviation of the gauge signal (open) for variations slower than 30 days, between 2 and 30 days and faster than 2 days.

default for version 3.0 with the quality flag used here. Because its advantage rests on one failure, this is not a general verdict on the denoising, which has to be assessed again at other coasts and for later product versions. The product documentation likewise takes the unfiltered anomaly as the base when it recommends adding the internal tide back (AVISO/DUACS, 2026). Pixels up to 6 km from a gauge agree with it as well as the nearest one, which supports the 5 km radius of Esselborn et al. (2025), but only 38% of the overpasses provide a valid pixel at the gauges used, so the inner coastal zone remains the domain of tide gauges.

4.2 Comparison with previous practice

The selected formula confirms what Baltic studies had assumed when they restored the DAC and kept the tide (Mostafavi et al., 2023, 2024; Esselborn et al., 2025). Agreement levels reported elsewhere reflect the basin and the frame of comparison as much as the altimeter. SWOT agrees with Baltic gauges to 4.73 cm in the anomaly frame, against 5.7 cm for Sentinel-3A along the Baltic coast with the DAC and the tide removed from the gauges (Sánchez-Román et al., 2020), about 13 cm for

https://doi.org/10.5194/egusphere-2026-7050
Preprint. Discussion started: 24 November 2026
© Author(s) 2026. CC BY 4.0 License.

Level-2 data against geoid-referenced Baltic gauges, which includes the datums (Kupavõh et al., 2024), 13–14 cm for total water level in the hyper-tidal Bristol Channel (Lichtman et al., 2025; Rong et al., 2026) and 0.19–0.32 m on the macro-tidal Jiangsu coast (Shi et al., 2025). Triple collocation gives a SWOT error of 4.14 cm here, against about 10 cm along the coasts of East Asia and the western United States (Zhu et al., 2025).

The test adds three things to previous practice. First, the coefficient β_X turns the choice into a quantity that can be measured with tide gauges for any altimeter, since nadir Level-3 products distribute the same variables (Pujol et al., 2023; E.U. Copernicus Marine Service Information, 2024), and the benefit $\sigma_X^2(2\beta_X - 1)$ shows why a small term such as the Baltic ocean tide still matters where the remaining error is small. Second, the result is specific to the basin. In the Baltic the DAC dominates the gain, with 113.66 against 18.39 cm^2 for the ocean tide, whereas in tide- or internal-tide-dominated regions the ranking is likely to be reversed (Hart-Davis et al., 2024; Tchilibou et al., 2025). Third, restoring the corrections in the altimetry and removing them from the reference are not equivalent once a model is involved. Removing the DAC from the gauges (Sánchez-Román et al., 2020; Zhu et al., 2025) leaves only its residual to compare, which in the Baltic is the smaller part of the signal, and removing it from a regional model would replace part of the model's own dynamics. Gauges and models also see the ocean tide relative to the sea floor, whereas `ocean_tide` is geocentric and includes the load tide (AVISO/DUACS, 2026). In the Baltic the coefficient of 1.00 shows no detectable effect, but in macro-tidal seas the load tide has to be treated separately (Lichtman et al., 2025).

4.3 What separates SWOT and the model

SWOT and the model have the same temporal variance, so the model reproduces the amplitude of Baltic sea level variability, and the differences lie in timing and spatial distribution. Its median hourly cRMSD against the gauges, 6.27 cm, is within the range reported for Nemo-Nordic (Kärnä et al., 2021). The cRMSD grows towards the coast while SWOT agrees with the gauges to 4.73 cm there, and the model error exceeds the SWOT error at the gauges, so this growth reflects mainly the model, which resolves coastlines, archipelagos and local wind set-up least well.

The constant offset combines the -5 cm offset of the MDT, the reference period of the mean sea surface and the zero level of the model, which has biases of tens of centimetres (Jahanmard et al., 2023; Jandt-Scheelke et al., 2024). The static field compares the MDT of the product with the mean sea level of the model, which differ by several centimetres along the Baltic (Ekman and Mäkinen, 1996; Jahanmard et al., 2021; Mostafavi et al., 2023). It cannot be attributed to either data set, but it makes up only one sixth of the difference.

Of the dominant uniform offset, 41% of the variance is model error that the tide gauges see independently of SWOT, and at the gauges the offset estimated from the other gauges of a sub-basin removes model error variance equivalent to a standard deviation of 4.08 cm ($\sqrt{6.35^2 - 4.87^2}$). Under the stronger assumptions of Sect. 3.5 the whole model part is at least 52%, so the gauges miss part of it. The model part reflects errors in the sea level of whole sub-basins from days to months, as produced by errors in the exchange through the Danish straits (Jakobsen et al., 2010), in the boundary sea level or in the large-scale wind set-up (Samuelsson and Stigebrandt, 1996; Leppäranta and Myrberg, 2009; Lorenz et al., 2025), which accumulate in the basin volume and persist until the exchange removes them (Jandt-Scheelke et al., 2024). This is consistent with the largest offsets

https://doi.org/10.5194/egusphere-2026-7050
Preprint. Discussion started: 24 November 2026
© Author(s) 2026. CC BY 4.0 License.

occurring from November to February, when persistent westerly storms fill the basin through the Danish straits (Leszczyńska et al., 2025), although storms may also enlarge the SWOT errors in these months. The remaining variance is SWOT error, including that of the re-injected corrections, together with any model error that the gauges miss. Only 2% of the variance of the offsets is linearly related to the DAC anomaly, so this is not mainly an error in the amplitude of the DAC, but it may contain other large-scale errors of the corrections or of KaRIn that remain after the calibration (Dibarboure et al., 2022). The residual part, 3.00 cm, is correlated over about 60 km and more than three times the uncorrelated SWOT noise, so it is a structured difference rather than instrument noise, largest near the coast and in the Skagerrak, Kattegat and western Baltic. Within a sub-basin SWOT has more spatial variance than the model at all separations, which points to sea level gradients that the model underestimates, but SWOT errors correlated across the swath (Dibarboure et al., 2022) would leave the same signature, and these data cannot separate the two.

4.4 Bias correction or data assimilation

A static bias correction does not bring the model close to SWOT, since it lowers the RMSD only from 7.21 to 6.66 cm. A time-varying offset from tide gauges, in the spirit of existing bias corrections and data-driven forecasts of Baltic sea level (Jahanmard et al., 2023; Rajabi-Kiasari et al., 2023; Barzandeh et al., 2025; Rajabi-Kiasari et al., 2025), lowers it to 5.29 cm. It explains 42% of the variance of the pass offsets, the same as the model error that the gauges see by triple collocation, so it removes what the gauges can see, and statistical corrections from more gauges add nothing. These are retrospective results (Sect. 2.6). In operation the offset could be computed at the analysis time from the gauges observed until then, whereas its benefit at forecast lead times depends on how long the offsets persist, and neither was evaluated here. The RMSD that remains contains the SWOT error itself. If the SWOT error at the gauges, 4.14 cm, which rests on the triple-collocation assumptions, also holds offshore and is independent of the model error, the model error left after the gauge-based offset is about 3.29 cm ($\sqrt{5.29^2 - 4.14^2}$), made of the sub-basin offsets that the gauges miss and of the model part of the structured residual. These are errors in the distribution of water between and within the sub-basins, which a dynamical correction through data assimilation could reduce and carry forward in time. We did not test assimilation, so this advantage is a hypothesis motivated by the structure of the errors.

The results indicate how such a test could be set up. The SWOT errors are smaller or larger than the model errors depending on the sub-basin (Sect. 3.5), so observation errors must be specified by region and checked in observation space (Desroziers et al., 2005). They contain representation error and are spatially correlated (Hollingsworth and Lönnberg, 1986; Oke and Sakov, 2008; Janjić et al., 2018), and part of the pass offsets is SWOT error, so the observation error needs a correlated component of a few centimetres, or a pass offset must be estimated with the model state. The static offset would be removed by referring SWOT to the model mean (Lellouche et al., 2018; Le Traon et al., 2025). SWOT observes a location about four times per 21-day cycle, whereas more than half of the model error at the gauges is local and faster than 2 days, which remains the domain of tide gauges (Madsen et al., 2015; Byrne et al., 2023). SWOT can add to the gauges only where it sees model error that they miss, which is the unseen part of the sub-basin offsets and, if it is model error, the structured residual. Swath altimetry has improved global forecasts by constraining scales unresolved by nadir altimetry (Benkiran et al., 2026), and data-driven reconstruction

https://doi.org/10.5194/egusphere-2026-7050
Preprint. Discussion started: 24 November 2026
© Author(s) 2026. CC BY 4.0 License.

from sparse observations (Lguensat et al., 2019; Elken et al., 2024; Kartal et al., 2024; Çelik et al., 2026), including SWOT in the Baltic (Rajabi-Kiasari et al., 2026), offers a complementary route.

In any case, the results cover three years and one model, a forecast without sea level assimilation. The negative gauge error variances in the Bothnian basins show that the independence assumed by triple collocation is not fully met there, possibly because the gauge and the model of the gauge cell share coastal effects that the SWOT pixel does not, but the covariance needed to remove them is small. SWOT errors uniform over a pass cannot be fully separated from model errors, and the model share depends on the assumptions stated in Sect. 2.7 and Sect. S1. Sea ice removes most SWOT samples in the northern basins in winter, so the winter results are dominated by the southern basins.

5 Conclusions

Using SWOT, tide gauges and a regional model together, this study diagnosed what their disagreement in the Baltic Sea consists of and what the satellite and the coastal observations each contribute, beyond how closely they agree. The diagnosis requires a SWOT sea level that is consistent with the model. In the Baltic this is the unfiltered Level-3 anomaly with the dynamic atmospheric correction and the ocean tide re-injected, $\eta_S = \mathrm{ssha_unfiltered} + \mathrm{dac} + \mathrm{ocean_tide}$. Written as a sum of switched terms, the formula shows that a correction improves the agreement with tide gauges only if the gauge residual regresses on it with a coefficient above one half, a test that can be repeated in any basin with tide gauges and the variables distributed with the product. In the Baltic the coefficients are 0.96 for the DAC and 1.00 for the ocean tide, and a similar result is expected in other microtidal, wind-driven seas, where the test can confirm it. The distributed internal tide correction is zero or undefined in the Baltic and has no numerical effect. The denoised anomaly agrees slightly better where it works but failed without a flag on one coastal pass, so the unfiltered anomaly is the robust default for the product version tested, though not a general verdict on the denoising, and pixels up to 6 km from a gauge agree with it as well as the nearest one.

SWOT and the Copernicus Marine Baltic forecast agree with a cRMSD of 6.60 cm and the same variance, and at the tide gauges triple collocation, which assumes independent errors, gives a SWOT error of 4.14 cm, smaller than that of the model, 5.50 cm. Apart from the datum, two thirds of their difference is an offset over each sub-basin that changes in time, one sixth a static offset field and one sixth a structured difference correlated over about 60 km. Of the time-varying offset, 41% is model error that the tide gauges also see, and if the SWOT and model errors are independent and the SWOT error over a pass is not larger than at a single pixel, the whole model part is at least 52%. A time-varying offset from the gauges removes the model error that they see, and the RMSD of 5.29 cm that remains contains about 3.29 cm of model error if the SWOT error at the gauges also holds offshore and is independent of the model error. The gauges thus constrain the sub-basin offsets continuously at the coast, whereas SWOT adds the offshore view of these offsets, including any part that the gauges miss, and the structured difference within sub-basins, although part of the latter may be SWOT error correlated across the swath.

The results of the present study provide a foundation for future efforts to use SWOT observations to correct or constrain regional shelf-sea models. Whether through data assimilation, data-driven corrections of the model state, or improvements in atmospheric and boundary forcing, such efforts benefit from three elements. First, a reconstruction of SWOT sea level

https://doi.org/10.5194/egusphere-2026-7050
Preprint. Discussion started: 24 November 2026
© Author(s) 2026. CC BY 4.0 License.

that is consistent with the physical processes represented by the model. Second, an assessment of the magnitude and spatial structure of observation–model discrepancies, including the relative contributions of SWOT and model errors and the spatially correlated observation errors associated with individual passes. Third, a retrospective benchmark established by conventional bias corrections, against which more advanced approaches can be evaluated with the information available at the analysis time and over the forecast lead times. This study addresses these requirements for the Baltic Sea and provides an evaluation framework that can be applied to other coastal and shelf seas where tide-gauge observations and regional model outputs are available.

Code and data availability. The SWOT Level-3 Expert data are available from AVISO (AVISO/DUACS, 2024), and the model and tide gauge data from the Copernicus Marine Data Store (E.U. Copernicus Marine Service Information, 2026a, b), under the DOIs given in Table 1. The Python code of the analysis and the result files behind the figures and tables are available on Zenodo (Nikbakhsh and Barzandeh, 2026).

Author contributions. All authors contributed to discussions and editing of the paper. **A.B.** and **P.L.** conceptualized the study. **N.N.** and **A.B.** developed the methodology, wrote the analysis software and carried out the formal analysis. **N.N.** carried out the investigation, prepared the figures and drafted the original manuscript. **A.B.** validated the results. **P.L.** provided resources. **P.L.** and **U.R.** acquired the funding, and supervised the study.

Competing interests. The authors declare that they have no conflict of interest.

Acknowledgements. The SWOT_L3_LR_SSH product, derived from the Level-2 SWOT KaRIn low rate ocean data products (L2_LR_SSH) (NASA/JPL and CNES), is produced and made freely available by AVISO and DUACS teams as part of the DESMOS Science Team project. During the preparation of this work the authors used Claude (Anthropic) to edit the text, check the consistency of numbers and references and assist with the analysis code. The authors reviewed and edited the content as needed and take full responsibility for the content of the published article.

Financial support. This study was carried out within the Estonian Coastal Monitoring and Forecasting Service 2025 project (No. 25339L02A-NCP USER DEMO-8000), funded by Mercator Ocean International and the Copernicus Marine Service through the Baltic Monitoring and Forecasting Centre, and the Baltic Monitoring and Forecasting Centre COP2 Phase 2 project (No. 24252L02-COP-MFC BAL-5200), funded by Mercator Ocean International.

https://doi.org/10.5194/egusphere-2026-7050
Preprint. Discussion started: 24 November 2026
© Author(s) 2026. CC BY 4.0 License.

References

Antony, C., Testut, L., and Unnikrishnan, A. S.: Observing storm surges in the Bay of Bengal from satellite altimetry, Estuarine, Coastal and Shelf Science, 151, 131–140, https://doi.org/10.1016/j.ecss.2014.09.012, 2014.

AVISO/DUACS: SWOT Level-3 KaRIn Low Rate SSH Expert (v3.0) [Data set], CNES, https://doi.org/10.24400/527896/A01-2023.018, 2024.

AVISO/DUACS: DUACS Level-3 SWOT KaRIn (L3_LR_SSH) User Handbook, Technical document SALP-MU-P-EA-23629-CLS, issue 3.2, CLS and CNES, https://www.aviso.altimetry.fr/en/data/product-information/aviso-user-handbooks.html, 2026.

Axell, L. and Liu, Y.: Application of 3-D ensemble variational data assimilation to a Baltic Sea reanalysis 1989–2013, Tellus A, 68, 24 220, https://doi.org/10.3402/tellusa.v68.24220, 2016.

Ballarotta, M., Ubelmann, C., Pujol, M.-I., Taburet, G., Fournier, F., Legeais, J.-F., Faugère, Y., Delepoulle, A., Chelton, D., Dibarboure, G., and Picot, N.: On the resolutions of ocean altimetry maps, Ocean Science, 15, 1091–1109, https://doi.org/10.5194/os-15-1091-2019, 2019.

Barzandeh, A., Ličer, M., Rus, M., Kristan, M., Maljutenko, I., Elken, J., Lagemaa, P., and Uiboupin, R.: Application of the HIDRA2 deep-learning model for sea level forecasting along the Estonian coast of the Baltic Sea, Ocean Science, 21, 1315–1327, https://doi.org/10.5194/os-21-1315-2025, 2025.

Benkiran, M., Fouchet, E., Le Traon, P.-Y., Remy, E., and Drillet, Y.: SWOT and swath altimetry: A breakthrough for global ocean prediction, Geophysical Research Letters, 53, e2025GL115 016, https://doi.org/10.1029/2025GL115016, 2026.

Byrne, D., Horsburgh, K., and Williams, J.: Variational data assimilation of sea surface height into a regional storm surge model: benefits and limitations, Journal of Operational Oceanography, 16, 1–14, https://doi.org/10.1080/1755876X.2021.1884405, 2023.

Carrère, L. and Lyard, F.: Modeling the barotropic response of the global ocean to atmospheric wind and pressure forcing – comparisons with observations, Geophysical Research Letters, 30, 1275, https://doi.org/10.1029/2002GL016473, 2003.

Carrere, L., Faugère, Y., and Ablain, M.: Major improvement of altimetry sea level estimations using pressure-derived corrections based on ERA-Interim atmospheric reanalysis, Ocean Science, 12, 825–842, https://doi.org/10.5194/os-12-825-2016, 2016.

Carrere, L., Arbic, B. K., Dushaw, B., Egbert, G., Erofeeva, S., Lyard, F., Ray, R. D., Ubelmann, C., Zaron, E., Zhao, Z., Shriver, J. F., Buijsman, M. C., and Picot, N.: Accuracy assessment of global internal-tide models using satellite altimetry, Ocean Science, 17, 147–180, https://doi.org/10.5194/os-17-147-2021, 2021.

Çelik, A., Mandev, M. B., and Altunkaynak, A.: Robust reconstruction of sea level fields from sparse observations using shallow recurrent decoders, Estuarine, Coastal and Shelf Science, 339, 109 978, https://doi.org/10.1016/j.ecss.2026.109978, 2026.

Cheng, Y., Xu, Q., and Li, X.: Spatio-temporal variability of annual sea level cycle in the Baltic Sea, Remote Sensing, 10, 528, https://doi.org/10.3390/rs10040528, 2018.

Cipollini, P., Calafat, F. M., Jevrejeva, S., Melet, A., and Prandi, P.: Monitoring sea level in the coastal zone with satellite altimetry and tide gauges, Surveys in Geophysics, 38, 33–57, https://doi.org/10.1007/s10712-016-9392-0, 2017.

CNES: FES2022 (Finite Element Solution) tidal model (Version 2024) [Data set], CNES, https://doi.org/10.24400/527896/A01-2024.004, 2024.

Demol, M., Ponte, A. L., Garreau, P., Bellacicco, M., Berta, M., Centurioni, L. R., Doglioli, A. M., Joël, A., Mourre, B., and Pascual, A.: Large drifter experiment in the Western Mediterranean Sea reveals dynamical versus noise contributions in SWOT-KaRIn sea level, Geophysical Research Letters, 53, e2025GL121 425, https://doi.org/10.1029/2025GL121425, 2026.

https://doi.org/10.5194/egusphere-2026-7050
Preprint. Discussion started: 24 November 2026
© Author(s) 2026. CC BY 4.0 License.

Desroziers, G., Berre, L., Chapnik, B., and Poli, P.: Diagnosis of observation, background and analysis-error statistics in observation space, Quarterly Journal of the Royal Meteorological Society, 131, 3385–3396, https://doi.org/10.1256/qj.05.108, 2005.

Dibarboure, G., Ubelmann, C., Flamant, B., Briol, F., Peral, E., Bracher, G., Vergara, O., Faugère, Y., Soulat, F., and Picot, N.: Data-driven calibration algorithm and pre-launch performance simulations for the SWOT mission, Remote Sensing, 14, 6070, https://doi.org/10.3390/rs14236070, 2022.

Dibarboure, G., Anadon, C., Briol, F., Cadier, E., Chevrier, R., Delepoulle, A., Faugère, Y., Laloue, A., Morrow, R., Picot, N., Prandi, P., Pujol, M.-I., Raynal, M., Tréboutte, A., and Ubelmann, C.: Blending 2D topography images from the Surface Water and Ocean Topography (SWOT) mission into the altimeter constellation with the Level-3 multi-mission Data Unification and Altimeter Combination System (DUACS), Ocean Science, 21, 283–323, https://doi.org/10.5194/os-21-283-2025, 2025.

Dufau, C., Orsztynowicz, M., Dibarboure, G., Morrow, R., and Le Traon, P.-Y.: Mesoscale resolution capability of altimetry: Present and future, Journal of Geophysical Research: Oceans, 121, 4910–4927, https://doi.org/10.1002/2015JC010904, 2016.

Efron, B. and Tibshirani, R. J.: An Introduction to the Bootstrap, Chapman & Hall/CRC, New York, https://doi.org/10.1201/9780429246593, 1993.

Ekman, M. and Mäkinen, J.: Mean sea surface topography in the Baltic Sea and its transition area to the North Sea: A geodetic solution and comparisons with oceanographic models, Journal of Geophysical Research: Oceans, 101, 11 993–11 999, https://doi.org/10.1029/96JC00318, 1996.

Elken, J., Barzandeh, A., Maljutenko, I., and Rikka, S.: Reconstruction of Baltic gridded sea levels from tide gauge and altimetry observations using spatiotemporal statistics from reanalysis, Remote Sensing, 16, 2702, https://doi.org/10.3390/rs16152702, 2024.

Esselborn, S., Schöne, T., Dobslaw, H., and Sulzbach, R.: The 2023 Major Baltic Inflow event observed by Surface Water and Ocean Topography (SWOT) and nadir altimetry, Remote Sensing, 17, 1289, https://doi.org/10.3390/rs17071289, 2025.

E.U. Copernicus Marine Service Information: European Seas Along-Track L3 Sea Level Anomalies Near Real Time, https://doi.org/10.48670/moi-00059, product ID: SEALEVEL_EUR_PHY_L3_NRT_008_059, 2024.

E.U. Copernicus Marine Service Information: Baltic Sea In Situ Near Real Time Observations, INSITU_BAL_PHYBGCWAV_DISCRETE_MYNRT_013_032, Copernicus Marine Data Store, https://doi.org/10.48670/moi-00032, 2026a.

E.U. Copernicus Marine Service Information: Baltic Sea Physics Analysis and Forecast, BALTICSEA_ANALYSISFORECAST_PHY_003_006, Copernicus Marine Data Store, https://doi.org/10.48670/moi-00010, 2026b.

Fennel, W., Seifert, T., and Kayser, B.: Rossby radii and phase speeds in the Baltic Sea, Continental Shelf Research, 11, 23–36, https://doi.org/10.1016/0278-4343(91)90032-2, 1991.

Fouchet, E., Benkiran, M., Le Traon, P.-Y., and Remy, E.: Comparison of a global high-resolution ocean data assimilation system with SWOT observations, Frontiers in Marine Science, 12, 1563 934, https://doi.org/10.3389/fmars.2025.1563934, 2025.

Fu, L.-L. and Ubelmann, C.: On the transition from profile altimeter to swath altimeter for observing global ocean surface topography, Journal of Atmospheric and Oceanic Technology, 31, 560–568, https://doi.org/10.1175/JTECH-D-13-00109.1, 2014.

Fu, L.-L., Pavelsky, T., Cretaux, J.-F., Morrow, R., Farrar, J. T., Vaze, P., Sengenes, P., Vinogradova-Shiffer, N., Sylvestre-Baron, A., Picot, N., et al.: The Surface Water and Ocean Topography mission: A breakthrough in radar remote sensing of the ocean and land surface water, Geophysical Research Letters, 51, e2023GL107 652, https://doi.org/10.1029/2023GL107652, 2024.

Fu, W., She, J., and Dobrynin, M.: A 20-year reanalysis experiment in the Baltic Sea using three-dimensional variational (3DVAR) method, Ocean Science, 8, 827–844, https://doi.org/10.5194/os-8-827-2012, 2012.

https://doi.org/10.5194/egusphere-2026-7050
Preprint. Discussion started: 24 November 2026
© Author(s) 2026. CC BY 4.0 License.

Han, G., Ma, Z., Chen, D., deYoung, B., and Chen, N.: Observing storm surges from space: Hurricane Igor off Newfoundland, Scientific Reports, 2, 1010, https://doi.org/10.1038/srep01010, 2012.

Han, G., Klymak, J. M., Ross, T., and Chen, N.: Validation of 1-day repeat SWOT measurements against tide-gauge and glider data off Canada's west coast, Geophysical Research Letters, 53, e2025GL119 491, https://doi.org/10.1029/2025GL119491, 2026.

Hart-Davis, M. G., Andersen, O. B., Ray, R. D., Zaron, E. D., Schwatke, C., Arildsen, R. L., Dettmering, D., and Nielsen, K.: Tides in complex coastal regions: early case studies from wide-swath SWOT measurements, Geophysical Research Letters, 51, e2024GL109 983, https://doi.org/10.1029/2024GL109983, 2024.

Hollingsworth, A. and Lönnberg, P.: The statistical structure of short-range forecast errors as determined from radiosonde data. Part I: The wind field, Tellus A, 38, 111–136, https://doi.org/10.1111/j.1600-0870.1986.tb00460.x, 1986.

Hordoir, R., Axell, L., Höglund, A., Dieterich, C., Fransner, F., Gröger, M., Liu, Y., Pemberton, P., Schimanke, S., Andersson, H., Ljungemyr, P., Nygren, P., Falahat, S., Nord, A., Jönsson, A., Lake, I., Döös, K., Hieronymus, M., Dietze, H., Löptien, U., Kuznetsov, I., Westerlund, A., Tuomi, L., and Haapala, J.: Nemo-Nordic 1.0: a NEMO-based ocean model for the Baltic and North seas – research and operational applications, Geoscientific Model Development, 12, 363–386, https://doi.org/10.5194/gmd-12-363-2019, 2019.

Jahanmard, V., Delpeche-Ellmann, N., and Ellmann, A.: Realistic dynamic topography through coupling geoid and hydrodynamic models of the Baltic Sea, Continental Shelf Research, 222, 104 421, https://doi.org/10.1016/j.csr.2021.104421, 2021.

Jahanmard, V., Hordoir, R., Delpeche-Ellmann, N., and Ellmann, A.: Quantification of hydrodynamic model sea level bias utilizing deep learning and synergistic integration of data sources, Ocean Modelling, 186, 102 286, https://doi.org/10.1016/j.ocemod.2023.102286, 2023.

Jakobsen, F., Hansen, I. S., Hansen, N.-E. O., and Østrup-Rasmussen, F.: Flow resistance in the Great Belt, the biggest strait between the North Sea and the Baltic Sea, Estuarine, Coastal and Shelf Science, 87, 325–332, https://doi.org/10.1016/j.ecss.2010.01.014, 2010.

Jandt-Scheelke, S., Panteleit, T., Verjovkina, S., Lagemaa, P., Spruch, L., and Morrison, H.: Quality Information Document for the Baltic Sea Physical Analysis and Forecasting Product BALTICSEA_ANALYSISFORECAST_PHY_003_006, Quality Information Document CMEMS-BAL-QUID-003-006, Copernicus Marine Service, https://data.marine.copernicus.eu/product/BALTICSEA_ANALYSISFORECAST_PHY_003_006/description, issue 8.0, 2024.

Janjić, T., Bormann, N., Bocquet, M., Carton, J. A., Cohn, S. E., Dance, S. L., Losa, S. N., Nichols, N. K., Potthast, R., Waller, J. A., and Weston, P.: On the representation error in data assimilation, Quarterly Journal of the Royal Meteorological Society, 144, 1257–1278, https://doi.org/10.1002/qj.3130, 2018.

Kärnä, T., Ljungemyr, P., Falahat, S., Ringgaard, I., Axell, L., Korabel, V., Murawski, J., Maljutenko, I., Lindenthal, A., Jandt-Scheelke, S., Verjovkina, S., Lorkowski, I., Lagemaa, P., She, J., Tuomi, L., Nord, A., and Huess, V.: Nemo-Nordic 2.0: operational marine forecast model for the Baltic Sea, Geoscientific Model Development, 14, 5731–5749, https://doi.org/10.5194/gmd-14-5731-2021, 2021.

Kartal, E., Altunkaynak, A., and Çelik, A.: Data-driven optimization of coastal sea level monitoring: Leveraging known patterns for enhanced reconstruction, Regional Studies in Marine Science, 80, 103 878, https://doi.org/10.1016/j.rsma.2024.103878, 2024.

Kollo, K. and Ellmann, A.: Geodetic reconciliation of tide gauge network in Estonia, Geophysica, 54, 27–38, https://www.geophysica.fi/article/geodetic-reconciliation-of-tide-gauge-network-in-estonia/, 2019.

Künsch, H. R.: The jackknife and the bootstrap for general stationary observations, The Annals of Statistics, 17, 1217–1241, https://doi.org/10.1214/aos/1176347265, 1989.

Kupavõh, A., Delpeche-Ellmann, N., Ellmann, A., and Soomere, T.: Examining the performance of satellite altimetry (SWOT) sea level data in the coastal areas of the Baltic Sea, Journal of Coastal Research, 113, 534–538, https://doi.org/10.2112/JCR-SI113-105.1, 2024.

https://doi.org/10.5194/egusphere-2026-7050
Preprint. Discussion started: 24 November 2026
© Author(s) 2026. CC BY 4.0 License.

Le Traon, P.-Y., Dibarboure, G., Lellouche, J.-M., Pujol, M.-I., Benkiran, M., Drevillon, M., Drillet, Y., Faugère, Y., and Remy, E.: Satellite altimetry and operational oceanography: from Jason-1 to SWOT, Ocean Science, 21, 1329–1347, https://doi.org/10.5194/os-21-1329-2025, 2025.

Lellouche, J.-M., Greiner, E., Le Galloudec, O., Garric, G., Regnier, C., Drevillon, M., Benkiran, M., Testut, C.-E., Bourdalle-Badie, R., Gasparin, F., Hernandez, O., Levier, B., Drillet, Y., Remy, E., and Le Traon, P.-Y.: Recent updates to the Copernicus Marine Service global ocean monitoring and forecasting real-time 1/12° high-resolution system, Ocean Science, 14, 1093–1126, https://doi.org/10.5194/os-14-1093-2018, 2018.

Leppäranta, M. and Myrberg, K.: Physical Oceanography of the Baltic Sea, Springer, Berlin, https://doi.org/10.1007/978-3-540-79703-6, 2009.

Leszczyńska, K., Alexanderson, H., Clemmensen, L. B., Giza, A., Lorenz, S., Moskalewicz, D., Oliński, P., Paprotny, D., Rosentau, A., Rutgersson, A., Stattegger, K., Szczuciński, W., Terefenko, P., Uścinowicz, G., Uścinowicz, S., and Wolski, T.: A review of storms and marine coastal flooding in the Baltic Sea – Insights from instrumental, historical and sedimentary record, Earth-Science Reviews, 266, 105 137, https://doi.org/10.1016/j.earscirev.2025.105137, 2025.

Lguensat, R., Huynh Viet, P., Sun, M., Chen, G., Fenglin, T., Chapron, B., and Fablet, R.: Data-driven interpolation of sea level anomalies using analog data assimilation, Remote Sensing, 11, 858, https://doi.org/10.3390/rs11070858, 2019.

Lichtman, I. D., Bell, P. S., Gommenginger, C., Banks, C., Calafat, F. M., Brown, J., and Williams, S. D. P.: Evaluating water levels from the Surface Water and Ocean Topography (SWOT) mission in a hyper-tidal coastal and estuarine environment, Earth and Space Science, 12, e2024EA004 104, https://doi.org/10.1029/2024EA004104, 2025.

Lindenthal, A., Ljungemyr, P., and Huess, V.: Product User Manual for the Baltic Sea Biogeochemical and Physical Analysis and Forecasting Products BALTICSEA_ANALYSISFORECAST_BGC_003_007 and BALTICSEA_ANALYSISFORECAST_PHY_003_006, Product User Manual CMEMS-BAL-PUM-003-006-007, Copernicus Marine Service, https://data.marine.copernicus.eu/product/BALTICSEA_ANALYSISFORECAST_PHY_003_006/description, issue 1.3, 2025.

Lorenz, M., Viigand, K., and Gräwe, U.: Untangling the waves: decomposing extreme sea levels in a non-tidal basin, the Baltic Sea, Natural Hazards and Earth System Sciences, 25, 1439–1458, https://doi.org/10.5194/nhess-25-1439-2025, 2025.

Lyard, F. H., Allain, D. J., Cancet, M., Carrère, L., and Picot, N.: FES2014 global ocean tide atlas: design and performance, Ocean Science, 17, 615–649, https://doi.org/10.5194/os-17-615-2021, 2021.

Madec, G., Bell, M., Benshila, R., Blaker, A., Bourdallé-Badie, R., Bricaud, C., Bruciaferri, D., Carneiro, D., Castrillo, M., Calvert, D., Chanut, J., Clementi, E., Coward, A., de Lavergne, C., Dobricic, S., Epicoco, I., Éthé, C., Fiedler, E., Ford, D., Furner, R., Ganderton, J., Graham, T., Harle, J., Hutchinson, K., Iovino, D., King, R., Lea, D., Levy, C., Lovato, T., Maisonnave, E., Mak, J., Castillo Sanchez, J. M., Martin, M., Martin, N., Martins, D., Masson, S., Mathiot, P., Mele, F., Mocavero, S., Moulin, A., Müller, S., Nurser, G., Oddo, P., Paronuzzi, S., Paul, J., Peltier, M., Person, R., Rousset, C., Rynders, S., Samson, G., Schroeder, D., Storkey, D., Storto, A., Téchené, S., Vancoppenolle, M., and Wilson, C.: NEMO Ocean Engine Reference Manual, https://doi.org/10.5281/zenodo.14515373, 2024.

Madsen, K. S., Høyer, J. L., and Tscherning, C. C.: Near-coastal satellite altimetry: Sea surface height variability in the North Sea–Baltic Sea area, Geophysical Research Letters, 34, L19 603, https://doi.org/10.1029/2007GL029965, 2007.

Madsen, K. S., Høyer, J. L., Fu, W., and Donlon, C.: Blending of satellite and tide gauge sea level observations and its assimilation in a storm surge model of the North Sea and Baltic Sea, Journal of Geophysical Research: Oceans, 120, 6405–6418, https://doi.org/10.1002/2015JC011070, 2015.

https://doi.org/10.5194/egusphere-2026-7050
Preprint. Discussion started: 24 November 2026
© Author(s) 2026. CC BY 4.0 License.

Männikus, R. and Soomere, T.: Directional variation of return periods of water level extremes in Moonsund and in the Gulf of Riga, Baltic Sea, Regional Studies in Marine Science, 57, 102 741, https://doi.org/10.1016/j.rsma.2022.102741, 2023.

Männikus, R., Soomere, T., and Viška, M.: Variations in the mean, seasonal and extreme water level on the Latvian coast, the eastern Baltic Sea, during 1961–2018, Estuarine, Coastal and Shelf Science, 245, 106 827, https://doi.org/10.1016/j.ecss.2020.106827, 2020.

McColl, K. A., Vogelzang, J., Konings, A. G., Entekhabi, D., Piles, M., and Stoffelen, A.: Extended triple collocation: Estimating errors and correlation coefficients with respect to an unknown target, Geophysical Research Letters, 41, 6229–6236, https://doi.org/10.1002/2014GL061322, 2014.

Medvedev, I. P., Rabinovich, A. B., and Kulikov, E. A.: Tides in three enclosed basins: The Baltic, Black, and Caspian seas, Frontiers in Marine Science, 3, 46, https://doi.org/10.3389/fmars.2016.00046, 2016.

Morrow, R., Fu, L.-L., Ardhuin, F., Benkiran, M., Chapron, B., Cosme, E., d'Ovidio, F., Farrar, J. T., Gille, S. T., Lapeyre, G., et al.: Global observations of fine-scale ocean surface topography with the Surface Water and Ocean Topography (SWOT) mission, Frontiers in Marine Science, 6, 232, https://doi.org/10.3389/fmars.2019.00232, 2019.

Mostafavi, M., Delpeche-Ellmann, N., Ellmann, A., and Jahanmard, V.: Determination of accurate dynamic topography for the Baltic Sea using satellite altimetry and a marine geoid model, Remote Sensing, 15, 2189, https://doi.org/10.3390/rs15082189, 2023.

Mostafavi, M., Ellmann, A., and Delpeche-Ellmann, N.: Long-term and decadal sea-level trends of the Baltic Sea using along-track satellite altimetry, Remote Sensing, 16, 760, https://doi.org/10.3390/rs16050760, 2024.

Müller, M., Homleid, M., Ivarsson, K.-I., Køltzow, M. A. Ø., Lindskog, M., Midtbø, K. H., Andrae, U., Aspelien, T., Berggren, L., Bjørge, D., et al.: AROME-MetCoOp: A Nordic convective-scale operational weather prediction model, Weather and Forecasting, 32, 609–627, https://doi.org/10.1175/WAF-D-16-0099.1, 2017.

Nikbakhsh, N. and Barzandeh, A.: Code and results for "Reconciling SWOT altimetry, tide gauges, and regional ocean models in the Baltic Sea", Zenodo, https://doi.org/10.5281/zenodo.24138021, 2026.

Noubissie, L. D., Birol, F., Onguene, R., Léger, F., Nino, F., and Naoussi, R. D.: Virtual coastal altimetry tide gauges along the West African coast, Estuarine, Coastal and Shelf Science, 296, 108 600, https://doi.org/10.1016/j.ecss.2023.108600, 2024.

Oke, P. R. and Sakov, P.: Representation error of oceanic observations for data assimilation, Journal of Atmospheric and Oceanic Technology, 25, 1004–1017, https://doi.org/10.1175/2007JTECHO558.1, 2008.

Pascual, A., Marcos, M., and Gomis, D.: Comparing the sea level response to pressure and wind forcing of two barotropic models: validation with tide gauge and altimetry data, Journal of Geophysical Research: Oceans, 113, C07 011, https://doi.org/10.1029/2007JC004459, 2008.

Passaro, M., Müller, F. L., Oelsmann, J., Rautiainen, L., Dettmering, D., Hart-Davis, M. G., Abulaitijiang, A., Andersen, O. B., Høyer, J. L., Madsen, K. S., et al.: Absolute Baltic Sea level trends in the satellite altimetry era: A revisit, Frontiers in Marine Science, 8, 647 607, https://doi.org/10.3389/fmars.2021.647607, 2021.

Picco, P., Vignudelli, S., and Repetti, L.: A comparison between coastal altimetry data and tidal gauge measurements in the Gulf of Genoa (NW Mediterranean Sea), Journal of Marine Science and Engineering, 8, 862, https://doi.org/10.3390/jmse8110862, 2020.

Pujol, M.-I., Faugère, Y., Taburet, G., Dupuy, S., Pelloquin, C., Ablain, M., and Picot, N.: DUACS DT2014: the new multi-mission altimeter data set reprocessed over 20 years, Ocean Science, 12, 1067–1090, https://doi.org/10.5194/os-12-1067-2016, 2016.

Pujol, M.-I., Dupuy, S., Vergara, O., Sánchez Román, A., Faugère, Y., Prandi, P., Dabat, M.-L., Dagneaux, Q., Lievin, M., Cadier, E., et al.: Refining the resolution of DUACS along-track Level-3 sea level altimetry products, Remote Sensing, 15, 793, https://doi.org/10.3390/rs15030793, 2023.

https://doi.org/10.5194/egusphere-2026-7050
Preprint. Discussion started: 24 November 2026
© Author(s) 2026. CC BY 4.0 License.

Rajabi-Kiasari, S., Delpeche-Ellmann, N., and Ellmann, A.: Forecasting of absolute dynamic topography using deep learning algorithm with application to the Baltic Sea, Computers & Geosciences, 178, 105 406, https://doi.org/10.1016/j.cageo.2023.105406, 2023.

Rajabi-Kiasari, S., Ellmann, A., and Delpeche-Ellmann, N.: Sea level forecasting using deep recurrent neural networks with high-resolution hydrodynamic model, Applied Ocean Research, 157, 104 496, https://doi.org/10.1016/j.apor.2025.104496, 2025.

Rajabi-Kiasari, S., Delpeche-Ellmann, N., Ellmann, A., and Zorita, E.: CDMSL: A conditional diffusion deep learning model for high-resolution sea level reconstruction using SWOT satellite altimetry, ESS Open Archive [preprint], https://doi.org/10.22541/essoar.15003713/v1, 2026.

Rong, Y., Bates, P., Neal, J., Bell, P., Gommenginger, C., Lichtman, I. D., et al.: Evaluating SWOT in the coastal zone: comparisons with tide gauge and airborne LiDAR in the Bristol Channel and Severn Estuary, UK, Geophysical Research Letters, 53, e2025GL116 590, https://doi.org/10.1029/2025GL116590, 2026.

Rulent, J., Calafat, F. M., Banks, C. J., Bricheno, L. M., Gommenginger, C., Green, J. A. M., Haigh, I. D., Lewis, H., and Martin, A. C. H.: Comparing water level estimation in coastal and shelf seas from satellite altimetry and numerical models, Frontiers in Marine Science, 7, 549 467, https://doi.org/10.3389/fmars.2020.549467, 2020.

Samuelsson, M. and Stigebrandt, A.: Main characteristics of the long-term sea level variability in the Baltic Sea, Tellus A, 48, 672–683, https://doi.org/10.3402/tellusa.v48i5.12165, 1996.

Sánchez-Román, A., Pascual, A., Pujol, M.-I., Taburet, G., Marcos, M., and Faugère, Y.: Assessment of DUACS Sentinel-3A altimetry data in the coastal band of the European seas: comparison with tide gauge measurements, Remote Sensing, 12, 3970, https://doi.org/10.3390/rs12233970, 2020.

Schwabe, J., Varbla, S., Ågren, J., Teitsson, H., Ellmann, A., Liebsch, G., Forsberg, R., Strykowski, G., Bilker-Koivula, M., Liepiņš, I., et al.: The development of the unified Baltic Sea Chart Datum 2000 (BSCD2000) height transformation grid: an unprecedented example of height system unification based on state-of-the-art marine geoid modelling, Journal of Geodesy, 100, 65, https://doi.org/10.1007/s00190-026-02096-z, 2026.

Shi, H., Jia, D., He, X., Andersen, O. B., and Zheng, X.: SWOT-based intertidal digital elevation model extraction and spatiotemporal variation assessment, Remote Sensing, 17, 1516, https://doi.org/10.3390/rs17091516, 2025.

Soomere, T., Eelsalu, M., and Pindsoo, K.: Variations in parameters of extreme value distributions of water level along the eastern Baltic Sea coast, Estuarine, Coastal and Shelf Science, 215, 59–68, https://doi.org/10.1016/j.ecss.2018.10.010, 2018.

Stoffelen, A.: Toward the true near-surface wind speed: Error modeling and calibration using triple collocation, Journal of Geophysical Research: Oceans, 103, 7755–7766, https://doi.org/10.1029/97JC03180, 1998.

Stramska, M.: Temporal variability of the Baltic Sea level based on satellite observations, Estuarine, Coastal and Shelf Science, 133, 244–250, https://doi.org/10.1016/j.ecss.2013.09.002, 2013.

Taburet, G., Sanchez-Roman, A., Ballarotta, M., Pujol, M.-I., Legeais, J.-F., Fournier, F., Faugere, Y., and Dibarboure, G.: DUACS DT2018: 25 years of reprocessed sea level altimetry products, Ocean Science, 15, 1207–1224, https://doi.org/10.5194/os-15-1207-2019, 2019.

Taylor, K. E.: Summarizing multiple aspects of model performance in a single diagram, Journal of Geophysical Research: Atmospheres, 106, 7183–7192, https://doi.org/10.1029/2000JD900719, 2001.

Tchilibou, M., Carrere, L., Lyard, F., Ubelmann, C., Dibarboure, G., Zaron, E. D., and Arbic, B. K.: Internal tides off the Amazon shelf in the western tropical Atlantic: analysis of SWOT Cal/Val mission data, Ocean Science, 21, 325–342, https://doi.org/10.5194/os-21-325-2025, 2025.

https://doi.org/10.5194/egusphere-2026-7050
Preprint. Discussion started: 24 November 2026
© Author(s) 2026. CC BY 4.0 License.

Tréboutte, A., Carli, E., Ballarotta, M., Carpentier, B., Faugère, Y., and Dibarboure, G.: KaRIn noise reduction using a convolutional neural network for the SWOT ocean products, Remote Sensing, 15, 2183, https://doi.org/10.3390/rs15082183, 2023.

Varbla, S., Ågren, J., Ellmann, A., and Poutanen, M.: Treatment of tide gauge time series and marine GNSS measurements for vertical land motion with relevance to the implementation of the Baltic Sea Chart Datum 2000, Remote Sensing, 14, 920, https://doi.org/10.3390/rs14040920, 2022.

Vega-Gimenez, D., Amores, A., Paris, A., and Pascual, A.: Expanding the coastal observation frontier: SWOT reveals the spatial footprint of storm surges, Geophysical Research Letters, 52, e2025GL117 299, https://doi.org/10.1029/2025GL117299, 2025.

Vignudelli, S., Birol, F., Benveniste, J., Fu, L.-L., Picot, N., Raynal, M., and Roinard, H.: Satellite altimetry measurements of sea level in the coastal zone, Surveys in Geophysics, 40, 1319–1349, https://doi.org/10.1007/s10712-019-09569-1, 2019.

Viigand, K., Eelsalu, M., and Soomere, T.: Quantifying exposedness of the eastern Baltic Sea shores with respect to extremely high and low water levels, Estuarine, Coastal and Shelf Science, 319, 109 267, https://doi.org/10.1016/j.ecss.2025.109267, 2025.

Wang, J., Lucas, A. J., Stalin, S., Lankhorst, M., Send, U., Schofield, O., Kachelein, L., Haines, B., Meinig, C., Pinkel, R., Farrar, J. T., and Fu, L.-L.: SWOT mission validation of sea surface height measurements at sub-100 km scales, Geophysical Research Letters, 52, e2025GL114 936, https://doi.org/10.1029/2025GL114936, 2025.

Weisse, R., Dailidienė, I., Hünicke, B., Kahma, K., Madsen, K., Omstedt, A., Parnell, K., Schöne, T., Soomere, T., Zhang, W., and Zorita, E.: Sea level dynamics and coastal erosion in the Baltic Sea region, Earth System Dynamics, 12, 871–898, https://doi.org/10.5194/esd-12-871-2021, 2021.

Yadidya, B., Arbic, B. K., Shriver, J. F., Zaron, E. D., Buijsman, M. C., Carrère, L., Tchilibou, M., and Uchida, T.: Advancing internal tide correction for SWOT Cal/Val: the role of ocean forecasts, Earth and Space Science, 12, e2025EA004 511, https://doi.org/10.1029/2025EA004511, 2025.

Zaron, E. D.: Baroclinic tidal sea level from exact-repeat mission altimetry, Journal of Physical Oceanography, 49, 193–210, https://doi.org/10.1175/JPO-D-18-0127.1, 2019.

Zaron, E. D. and Elipot, S.: Estimates of baroclinic tidal sea level from Lagrangian drifters and satellite altimetry, Journal of Atmospheric and Oceanic Technology, 41, 781–802, https://doi.org/10.1175/JTECH-D-23-0159.1, 2024.

Zhai, L., Lu, Y., Hu, X., and Dupont, F.: Evaluating model-simulated monthly sea levels during 1993–2023 in the Northwest Atlantic: influence of model resolution and data assimilation, Journal of Marine Science and Engineering, 13, 2379, https://doi.org/10.3390/jmse13122379, 2025.

Zhu, H., Peng, F., and Shen, Y.: Validation of sea level anomalies from the SWOT altimetry mission around the coastal regions of East Asia and the US West Coast, Water, 17, 3066, https://doi.org/10.3390/w17213066, 2025.